



A NIRS–fMRI study of resting state network

Shuntaro Sasai^{a,b,*}, Fumitaka Homae^c, Hama Watanabe^a, Akihiro T. Sasaki^{b,d,e}, Hiroki C. Tanabe^{d,e}, Norihiro Sadato^{d,e,f}, Gentaro Taga^a

^a Graduate School of Education, The University of Tokyo, Tokyo, 7-3-1 Hongo, Bunkyo-ku, Tokyo 113-0033, Japan

^b Japan Society for the Promotion of Science, Sumitomo-Ichibancho FS Bldg., 8 Ichibancho, Chiyoda-ku, Tokyo 102-8472, Japan

^c Department of Language Sciences, Tokyo Metropolitan University, 1-1 Minami Osawa, Hachioji, Tokyo 192-0397, Japan

^d Division of Cerebral Integration, Department of Cerebral Research, National Institute for Physiological Sciences, 38, Nishigo-naka, Myodaiji, Okazaki, Aichi 444-8585, Japan

^e Department of Physiological Sciences, The Graduate University for Advanced Studies (Sokendai), 38, Nishigo-naka, Myodaiji, Okazaki, Aichi 444-8585, Japan

^f Japan Science and Technology Agency/Research Institute of Science and Technology for Society, K's Gobancho Bldg, 7, Gobancho, Chiyoda-ku, Tokyo 102-0076, Japan

ARTICLE INFO

Article history:

Accepted 8 June 2012

Available online 17 June 2012

Keywords:

Resting state

Functional connectivity

Resting state network

Default mode network

Simultaneous NIRS–fMRI recording

Spontaneous hemodynamic fluctuation

ABSTRACT

Resting state functional connectivity, which is defined as temporal correlation of spontaneous activity between diverse brain regions, has been reported to form resting state networks (RSNs), consisting of a specific set of brain regions, based on functional magnetic resonance imaging (fMRI). Recently, studies using near-infrared spectroscopy (NIRS) reported that NIRS signals also show temporal correlation between different brain regions. The local relationship between NIRS and fMRI signals has been examined by simultaneously recording these signals when participants perform tasks or respond to stimuli. However, the NIRS–fMRI signal relationship during the resting state has been reported only between NIRS signals obtained within limited regions and whole brain fMRI signals. Therefore, it remains unclear whether NIRS signals obtained at diverse regions correlate with regional fMRI signals close to the NIRS measurement channels, especially in relation to the RSNs. In this study, we tested whether the signals measured by these different modalities during the resting state have the consistent characteristics of the RSNs. Specifically, NIRS signals during the resting state were acquired over the frontal, temporal, and occipital cortices while whole brain fMRI data was simultaneously recorded. First, by projecting the NIRS channel positions over the cerebral cortical surface, we identified the most likely anatomical locations of all NIRS channels used in the study. Next, to investigate the regional signal relationship between NIRS and fMRI, we calculated the cross-correlation between NIRS signals and fMRI signals in the brain regions adjacent to each NIRS channel. For each NIRS channel, we observed the local maxima of correlation coefficients between NIRS and fMRI signals within a radius of 2 voxels from the projection point. Furthermore, we also found that highly correlated voxels with the NIRS signal were mainly localized within brain tissues for all NIRS channels, with the exception of 2 frontal channels. Finally, by calculating the correlation between NIRS signals at a channel and whole brain fMRI signals, we observed that NIRS signals correlate with fMRI signals not only within brain regions adjacent to NIRS channels but also within distant brain regions constituting RSNs, such as the dorsal attention, fronto-parietal control, and default mode networks. These results support the idea that NIRS signals obtained at several cortical regions during the resting state mainly reflect regional spontaneous hemodynamic fluctuations that originate from spontaneous cortical activity, and include information that characterizes the RSNs. Because NIRS is relatively easy to use and a less physically demanding neuroimaging technique, our findings should facilitate a broad application of this technique to examine RSNs, especially for clinical populations and conditions unsuitable for fMRI.

© 2012 Elsevier Inc. All rights reserved.

Introduction

The brain typically operates in a coordinated manner even during the resting state. Functional magnetic resonance imaging (fMRI)

demonstrates that there is a strong correlation among blood oxygenation level-dependent (BOLD) signal fluctuations of distinct regions of the brain in the low-frequency range (<0.1 Hz) in the resting state (Biswal et al., 1995). This correlation, termed resting state functional connectivity, has often been observed between functionally related brain regions, including sensory, motor, sensory association, attention, and task-negative regions (Fox and Raichle, 2007). When we regard this connectivity as the “edge” and the brain regions linked by the connectivity as the “node,” the spontaneous brain activity constitutes unique network architectures, termed resting state networks

* Corresponding author at: Division of Physical and Health Education, Graduate school of Education, University of Tokyo, 7-3-1, Hongo, Bunkyo-ku, Tokyo 113-0033, Japan. Fax: +81 3 5841 1396.

E-mail address: sasai@p.u-tokyo.ac.jp (S. Sasai).

(RSNs) (De Luca et al., 2006; Fox and Raichle, 2007; Lowe et al., 1998). These network architectures are consistent across healthy individuals (Damoiseaux et al., 2006), and are suggested to reflect intrinsic functional architecture of the brain (Fox and Raichle, 2007).

Near-infrared spectroscopy (NIRS) is a technique for measuring changes in local oxygenated and deoxygenated hemoglobin (oxy-Hb and deoxy-Hb) concentrations. Studies using NIRS have successfully observed functional connectivity during the resting state in both adult and infant participants (Homae et al., 2010, 2011; Lu et al., 2010; Mesquita et al., 2010; White et al., 2009; Zhang et al., 2010). One NIRS study also demonstrated that functional connectivity estimated using oxy-Hb and deoxy-Hb signals obtained during the resting state has different frequency characteristics (Sasai et al., 2011). Moreover, higher temporal resolution of NIRS has revealed a temporal relationship of signals obtained at different brain regions in combination with analysis of phase synchronization (Taga et al., 2000, 2011). These results support that NIRS is a useful neuroimaging technique for acquisition of information about functional connectivity. Considering that NIRS is less physically demanding and relatively easy to use compared to other neuroimaging techniques, application of NIRS may allow easy RSN data collection even in cases where fMRI would be difficult to use.

Because both fMRI and NIRS signals measured during the resting state may reflect spontaneous brain activity, NIRS signals in diverse regions of the cortex during the resting state should show a high correlation with BOLD signals in regions adjacent to each of the NIRS measurement positions. Furthermore, despite the fact that NIRS can detect cortical activity only in superficial cortical regions, we can hypothesize that the NIRS signals measured in separate regions of the cortex can capture information reflecting different RSNs that include not only superficial regions, but also deep brain regions such as the default mode network (Buckner et al., 2008; Raichle et al., 2001). However, although the simultaneous use of these techniques during stimulation or task execution has shown a high correlation between the 2 different signals in the corresponding cortical regions (Cui et al., 2011; Hoge et al., 2005; Kleinschmidt et al., 1996; Schroeter et al., 2006; Strangman et al., 2002; Toronov et al., 2001; Toyoda et al., 2008), it is not well understood whether this relationship is also true during the resting state. Moreover, although previous studies have simultaneously recorded NIRS signals within limited regions and BOLD signals of the whole brain during the resting state (Duan et al., 2012; Tong and Frederick, 2010), the investigators did not compare the NIRS signals in diverse regions of the cortex and the BOLD signals. Thus, the aim of this study was to establish the NIRS–fMRI relationship to study functional connectivity with special focus on the RSNs.

To solve the above-mentioned issue, we designed and conducted step-by-step analyses. First, we had to determine the relative locations of NIRS measurement channels on the participant's brain to determine the brain regions where NIRS acquires its signals. However, we could obtain only the probabilistic anatomical cranio-cerebral correlation to represent the anatomical location of NIRS measurement channels (Okamoto et al., 2004), because NIRS probes are located outside of the head. Thus, we obtained structural MRI of all participants while they were wearing NIRS probes and determined the accurate positional relationships between their brain regions and the NIRS probes, which constituted 14 channels and were located on bilateral frontal, temporal, and occipital cortices.

Second, we aimed to confirm that NIRS signals obtained at a channel during the resting state reflected the spontaneous hemodynamic fluctuations within the adjacent brain regions. Previous studies of simultaneous recording of NIRS and fMRI have revealed that NIRS signals induced by several stimuli show high correlation with the BOLD signals obtained from adjacent brain regions to the NIRS measurement channels (Cui et al., 2011; Hoge et al., 2005; Kleinschmidt et al., 1996; Schroeter et al., 2006; Strangman et al., 2002; Toronov et al., 2001; Toyoda et al., 2008). In theory, with or without tasks, NIRS signals should reflect the concentration changes of oxy-Hb and deoxy-Hb

within close regions to NIRS channels. However, this theoretical deduction has not been confirmed for NIRS signals obtained during the resting state. To test this, we investigated whether we could find the local maximum of correlation coefficients between NIRS and BOLD signals simultaneously obtained during the resting state in the brain region close to each NIRS channel. However, because photons travel in a “banana shape” between the emitter and the detector (Okada et al., 1997; van der Zee et al., 1990), NIRS signals can be affected not only by changes in hemoglobin concentration within adjacent brain regions but also by those changes within non-brain regions such as skin and large pial veins (Gagnon et al., 2012a, 2012b; Kohno et al., 2007; Obrig et al., 2000; Saager and Berger, 2008; Tachtsidis et al., 2008; Takahashi et al., 2011; Tonorov et al., 2000; Yamada et al., 2009; Zhang et al., 2007). Therefore, to evaluate whether the concentration changes of oxy-Hb and deoxy-Hb in the brain tissues are major substitutes of the NIRS signals obtained during the resting state, we sorted highly correlating voxels with NIRS signals by tissue types of the voxels (gray matter, white matter, cerebrospinal fluid [CSF], skull and skin), and calculated the proportion of the voxels within brain tissues (gray and white matter) against those within non-brain tissues (skull and skin).

Finally, we aimed to clarify whether RSNs estimated using fMRI data sets could be reproduced using NIRS signals. One of the techniques to estimate RSNs in the fMRI data sets is based on the calculation of cross-correlation between a BOLD time-course extracted from a region of interest (ROI) as a seed and those of whole brain voxels. If NIRS signals include information characterizing RSNs contained in the seed BOLD signals, RSNs estimated using the BOLD signals extracted from ROIs should be reproduced using NIRS signals obtained from the ROIs. Thus, we investigated this issue by calculating correlation maps using BOLD and corresponding NIRS signals as seed signals.

If NIRS signals obtained from diverse regions of the cortex are probed to reflect the time-series characterizing the major RSNs obtained by fMRI, it becomes possible to acquire the time-series that represents RSNs solely by conducting NIRS measurement of the selected regions of the brain. By taking advantage of the high temporal resolution, we can address the temporal relationship between different RSNs (Chang and Glover, 2010; Kang et al., 2011; Majeed et al., 2011) using NIRS. Considering that NIRS measurement is relatively easy to use and a less physically demanding neuroimaging technique, application of NIRS would facilitate collection of data on the RSNs not only in normal experimental environments but also in other situations such as those involving a whole sleep period or social interaction, and in particular populations such as infants and patients. Thus, using the above-mentioned step-by-step analyses, we investigated whether sparse NIRS signals obtained from diverse regions of the cortex can represent the time-series for major RSNs obtained by fMRI.

Materials and methods

The outline of the analysis conducted in this study is shown in Fig. 1.

Participants

Twenty-eight healthy adults (15 men and 13 women; age range, 22–44 years) participated in this study. All participants were awake with their eyes closed during the measurement. The protocol was approved by the ethical committee of the National Institute for Physiological Sciences, Okazaki, Japan. Informed consent was obtained from all participants prior to initiation of the experiments.

Data acquisition

NIRS

We used a near-infrared optical topography instrument (ETG-4000; Hitachi Medical Corporation, Tokyo, Japan) to measure the

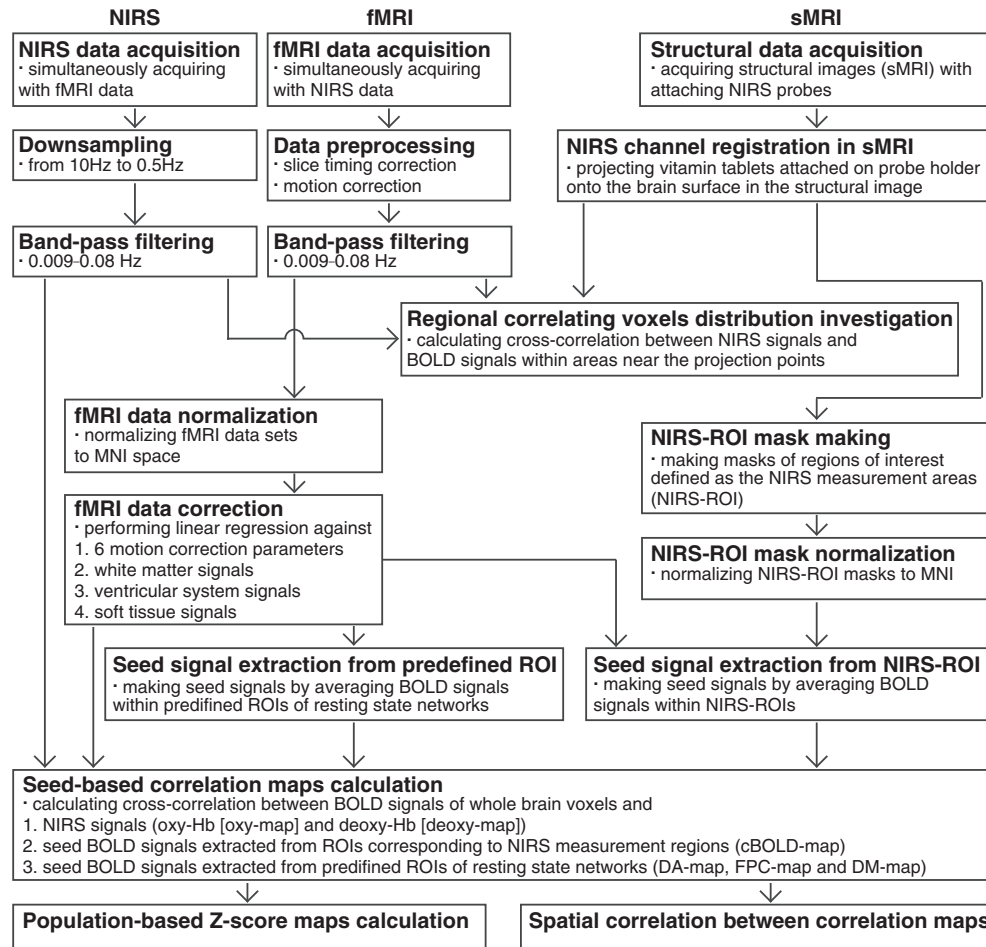


Fig. 1. Outline of all analyses conducted in the current study.

time-courses of spontaneous changes in oxy-Hb and deoxy-Hb during a 20-min period with 0.1-s time resolution (Fig. 1, “NIRS data acquisition”). The instrument generated 2 wavelengths of near-infrared light (695 nm and 830 nm). We evaluated relative changes in the oxy-Hb and deoxy-Hb signals from an arbitrary baseline (set to 0) at the beginning of the measurement period based on the Lambert–Beer law. The unit used to measure these values was molar concentration multiplied by length (mM·mm). The distance between the incident and the detection fibers was 3 cm. The 8 emitters and 8 detectors were plugged into a holder, on which vitamin tablets were attached to identify the positions of NIRS channels in MRI images (Fig. 2A), and were arranged into two 1×8 arrays, resulting in 14 measurement channels (Fig. 2B). Arrays were positioned over the bilateral frontal, temporal and occipital regions by referring to the international 10–20 System of Electrode Placement (Fig. 2C). NIRS data were simultaneously obtained with functional MRI imaging for all participants, with each participant lying supine in an MRI scanner. The appearance of simultaneous recording with NIRS and fMRI is shown in Fig. 2D. A pillow was placed under the occiput to fix the participant’s head and to avoid compressing the NIRS probes (Fig. 2E).

MRI

Functional and structural MRI images were acquired using a 3-Tesla MR scanner (Allegra; Siemens; Fig. 1, “fMRI data acquisition” and “Structural data acquisition”). First, a time-series of 610 volumes was acquired for each session using T2*-weighted gradient-echo echo-planar imaging (EPI) sequence. Each volume consisted of 34 slices, each of which was 3.5 mm thick, with a 17% gap. The time interval between 2 successive acquisitions of the same slice (TR) was 2000 ms

with a flip angle (FA) of 76° and an echo time (TE) of 30 ms. The field of view (FoV) was 192×192 mm and the in-plane matrix size was 64×64 pixels. Additionally, to acquire a fine structural whole brain image, magnetization-prepared rapid-acquisition gradient-echo (MP-RAGE) images were obtained (TR = 2500 ms; TE = 4.38 ms; FA = 8° ; FoV = 230×230 mm; one slab; number of slices per slab = 192; voxel dimensions = $0.9 \times 0.9 \times 1.0$ mm).

Data preprocessing

NIRS

Both oxy-Hb and deoxy-Hb signals were downsampled to the fMRI acquisition frequency of 0.5 Hz by applying an anti-aliasing (lowpass) FIR filter in MATLAB (MathWorks, Inc., Natick, MA, USA) because these signals were measured with a 20-times higher sampling rate an fMRI data sets (10 Hz; Fig. 1, “Downsampling”). Spontaneous low-frequency fluctuations are contaminated by various other signals originating mainly from non-neural sources. To remove the long-term trends, respiratory and cardiac noises that are generally included outside the frequency band, we used a Butterworth band-pass filter (0.009–0.08 Hz) and performed zero-phase digital filtering by processing the data in both the forward and reverse directions in MATLAB (Fig. 1, “Band-pass filtering”).

fMRI

Functional MRI volumes were motion-corrected and slice-timing corrected using the SPM8 package (Wellcome Department of Imaging Neuroscience, London, UK) (Fig. 1, “Data preprocessing”). These functional volumes were not spatially smoothed nor normalized.

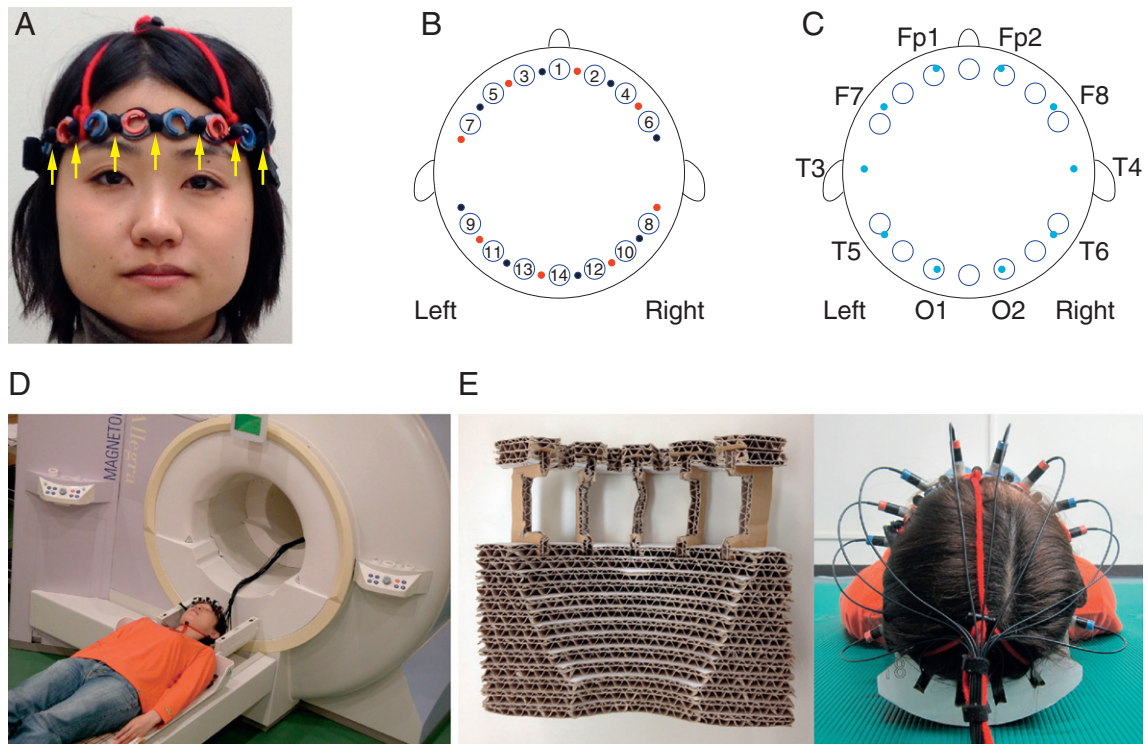


Fig. 2. Experimental conditions, materials, and channel configuration. (A) Probe holder. Yellow arrows indicate attached vitamin tablets (black balls). (B) Configuration of emitters (red dots), detectors (black dots), and measurement channels (blue circles) of the NIRS system. Each channel was indexed by its unique number. (C) Configuration of 14 measurement channels (blue circles) of NIRS based on the international 10–20 system (cyan dots). (D) Appearance of simultaneous recording with NIRS and fMRI. (E) Pillow used to fix the participant's head in the MRI scanner and to avoid compressing NIRS probes.

Subsequently, all data sets were processed with the same band-pass filter that was applied to NIRS signals (Fig. 1, “Band-pass filtering”).

Registration of NIRS channels in the structural MRI

We defined projection points from each vitamin tablet onto the brain surface as the locations of each NIRS channel (Fig. 1, “NIRS channel registration in sMRI”). Simulation studies demonstrated that we can assume that the photon-traveling pathways are a “banana” shape between the incident and detection probes (Okada et al., 1997; van der Zee et al., 1990). Taking into account this property, the projection points were determined as follows. First, by visually searching vitamin tablets in the structural MRI images (Fig. 3A),

we manually identified the position of each tablet in the structural image of each participant. Second, as shown in Fig. 3B, to determine a plane that mostly includes optical paths from the emitter to the detector for a NIRS channel, an optical path plane was estimated using a corresponding tablet and the 2 adjacent tablets on both sides. This plane was determined by minimizing a sum of squares of the distances between the plane and all voxels inside the 3 tablets. This procedure was used to determine planes for channels 1–5 and 10–14, whereas a plane for an adjacent channel was used for channels 6–9. Third, to determine a projection line from the position of a tablet to the cortical surface, a bisector of the angle formed by the 3 median points of the section of the tablets on the optical path plane was chosen as a projection line for channels 1–5 and 10–14. On the

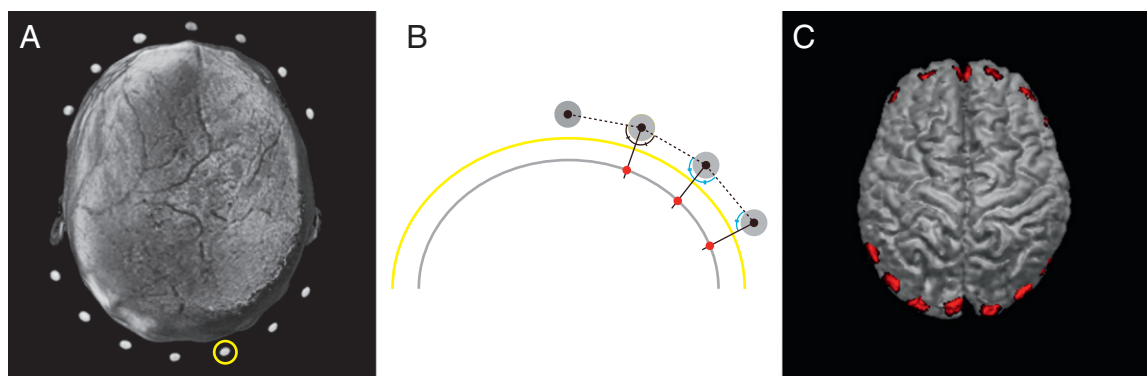


Fig. 3. Determination of the cortical positions of vitamin tablets representing NIRS channels on the head. (A) Representative example of a structural image. One of 14 vitamin tablets is surrounded by the open yellow circle. (B) Determination of the cortical projection points of vitamin tablets. Yellow and grey lines represent the skull and brain surfaces, respectively. Red dots are the determined projection points. Projection points were determined by projecting bisectors (black lines) of the angle formed by the 3 median points (black dots) of the section of the tablets on the optical path plane (filled grey circles) to the cortical surface. Angles with the same color have the same measure (black and cyan). (C) Representative example of determined ROIs corresponding to NIRS channels in the structural image. Red regions represent ROIs.

other hand, by assuming that the curvature of the probe holder is constant along channels 4 and 6 and channels 5 and 7, a projection line was determined using the bisector angle and the plane of the adjacent channel for channels 6–9. Fourth, the projection point for each NIRS channel was defined as the intersection of the projection line of each channel and the surface of a gray matter mask, which was estimated from the structural image of each participant using the segmentation tool in SPM8.

After the projection points were determined for all channels in each individual's data set by the above-mentioned procedure, we calculated the Montreal Neurological Institute (MNI) coordinates of the projection points. Subsequently, the mean and standard deviation of the MNI coordinates across all participants was calculated for each channel. Automated anatomical labeling (AAL) was applied to the mean MNI coordinate of each channel to obtain the most likely estimate (Tzourio-Mazoyer et al., 2002). We also applied the AAL system to the MNI coordinate of each channel in the data for each individual, and evaluated the anatomical variability of a channel position across all participants.

Evaluation of regions where hemodynamic fluctuations were detected as NIRS signals during the resting state

We aimed to investigate the regions where hemodynamic fluctuations are detected as NIRS signals obtained during the resting state by finding the correlated voxels in the simultaneously acquired fMRI data (Fig. 1, “Regional correlating voxels distribution investigation”). A previous study using multiple tasks showed that NIRS signals mainly correlate with BOLD signals of the voxels adjacent to the projection points of channel markers located between emitters and detectors attached to the brain surfaces (Cui et al., 2011). Therefore, we assumed that NIRS signals should detect hemodynamics fluctuating in adjacent regions to the projection points of vitamin tablets for all measurement channels, even if there were many correlated voxels with NIRS signals distributing across broad brain regions. From this point of view, we identified the local best-correlated voxels (LBCV) with NIRS signals (Cui et al., 2011), and investigated the spatial distributions of correlating voxels around the probe positions.

Distribution of the LBCV by referring the projection point

After the preprocessing step, fMRI data sets were coregistered with the structural image of each participant using DARTEL in SPM8 (Ashburner, 2007). Subsequently, we calculated the cross-correlation between each Hb signal obtained at each channel and BOLD signals from the whole head voxels. For each measurement channel, we identified the nearest voxel from the projection point that satisfied the following 2 conditions: (1) the correlation value for the voxel had a local maximum and (2) the correlation value was above 0.1 (Cui et al., 2011). Subsequently, we calculated the distance between the projection point and LBCV for each measurement channel.

Tissue level distribution

Because photons may travel across several tissues of a participant's head, highly correlated voxels (HCV) with NIRS signals can be located outside of the brain tissues. To investigate whether HCVs were located within the brain tissues, we identified the tissue type of HCVs. To do so, we estimated the mask of the brain tissue and the non-brain tissue using the New Segmentation method prepared in SPM8. By applying this method to the individual structural images, 6 types of masks were used (grey matter, white matter, CSF, skull, soft tissue, and air/background). Therefore, by combining the coregistered masks, we divided the voxels of fMRI data into 2 types of tissues: (1) brain tissue consisting of grey and white matter, and (2) non-brain tissue consisting of skull and soft tissue. After all, we investigated the locations of the top 100 ranked voxels within a 3-cm radius from the

projection points and identified the types of tissues (brain tissue and non-brain tissue) of these voxels.

Whole brain distribution of correlated voxels with NIRS signals obtained during the resting state

After investigating the local relationship between NIRS and fMRI signals, we focused on examination of the spatial distribution of correlated voxels over the whole brain. Because fMRI studies have repeatedly reported the existence of specific patterns of correlated voxels among several spatially separated brain regions, the NIRS signal can also correlate with BOLD signals from voxels other than those in adjacent areas to the channel. Therefore, we investigated whether the NIRS signal obtained at each measurement channel consistently reproduced the spatial pattern of the seed-based correlation map calculated with the BOLD signal of the regions of interest (ROI) corresponding to that NIRS measurement region. Furthermore, some NIRS probes were located near the brain regions included in the sets of brain regions specific to some RSNs (dorsal attention [DA], fronto-parietal control [FPC], and default mode [DM] networks), which have been reported consistently across various fMRI studies. Therefore, we also focused on determination of whether the NIRS signal obtained near the brain regions specific to the RSN determined the consistent RSN across participants.

Noise signal regression

After the above preprocessing steps, fMRI data sets were normalized to the MNI space using DARTEL in SPM8 (Fig. 1, “fMRI data normalization”). It is known that some types of noises are included in BOLD signals within the pass band of a band-pass filter (0.009–0.08 Hz). Therefore, multi-regression analysis was conducted to eliminate residual noises within the pass band of the filter from the fMRI data sets (Fig. 1, “fMRI data correction”). Generally, fluctuations due to scanner instabilities, subject motion and respiration and cardiac effects, the coherent signal fluctuations across the brain (global signal) are considered to contaminate BOLD signals in the frequency band. In many studies, these contaminating signals are estimated by utilizing MRI data-inherent information and removed using a general linear model (GLM) technique (Fox et al., 2005). However, the regression of the global signal has been shown to introduce spurious anti-correlated RSNs (Anderson et al., 2011; Murphy et al., 2009). To avoid this, Anderson et al. proposed an alternate method for correcting the global signal that makes use of an optimally phase-shifted waveform extracted from soft tissues of the face and calvarium, as well as regressors obtained from subject motion parameters, white matter, ventricle and physiological waveforms (method termed phase-shifted soft tissue correction [PSTCor]). To avoid generating spurious anti-correlation, in this study we also applied phase-shifted soft tissue time-series as a regressor for the global signal correction instead of using the global signal. Although the original method proposed by Anderson et al. included some additional physiological waveforms, we selected 18 components for the regressors by estimating the following procedures:

1. Signals within white matters: These signals are largely independent from BOLD signal changes in cortical and sub-cortical gray matter, but exhibit fluctuations due to scanner instabilities, subject motion, and respiration (Windischberger et al., 2002). We applied the white matter time-series as a nuisance regressor and obtained it from the mean time-series of voxels within 2 bounding boxes in each hemisphere of each participant defined by MNI coordinates (left hemisphere: $-38 < x < -28$, $-23 < y < -13$, $26 < z < 35$; right hemisphere: $28 < x < 38$, $-23 < y < -13$, $26 < z < 35$) that were determined based on the method used in a previous report (Fox et al., 2009).

2. Signals within ventricle: Physiological artifacts including respiration and cardiac effects are also present in the CSF (Dagli et al., 1999; Windischberger et al., 2002). After normalizing the functional images of all participants into the MNI space, we identified voxels commonly contained in CSF-segmented images made by SPM8 for all participants. Among these voxels, we selected those within the anterior horn of the lateral ventricle, and extracted the regressor as the mean time-series within the selected voxels.
3. Signals within soft tissues: Soft tissue time-series was applied as a regressor to correct the coherent signal fluctuations across the brain. The soft tissue restriction mask was created for each participant to contain voxels within the face and calvarium.
- 4–9. Time-series of motion correction parameters: In addition to the 3 aforementioned regressors, we also applied the time-series of motion parameters from the automated realignment procedure (realign step from preprocessing described above) as nuisance regressors. Three of 6 correspond to parameters of x, y and z translation, whereas the other 3 correspond to those of x, y and z rotation.
- 10–18. The temporal derivatives of the upper 9 components were used.

Before processing functional data sets with these 18 regressors, the first 3 time-series of regressors were phase shifted to achieve optimal correlation with the mean gray matter signal (Anderson et al., 2011). After these 3 signals were phase shifted, temporal derivatives of 1–3 were also prepared to achieve optimal correlation with the mean gray matter signal. No phase shifting was performed for motion parameters because these were measured at zero lag from image data and showed the highest correlation coefficients at the lag. Finally, these 18 parameters were regressed out from filtered BOLD time-series of all voxels using a GLM technique.

Estimation of correlation maps

We estimated the 3 types of seed-based correlation maps calculated with different seed signals:

1. NIRS (oxy-Hb and deoxy-Hb) time-series: Both preprocessed oxy-Hb and deoxy-Hb signals of all channels were used.
2. BOLD time-series extracted from the brain regions selected as corresponding voxels to NIRS measurement regions in each participant's structural image: We estimated 14 ROIs corresponding to the NIRS measurement channels in each participant's structural image to obtain the corresponding BOLD time-series to the NIRS signals (Fig. 1, "NIRS-ROI mask making"). Because NIRS signals, in theory, are generated by changes in the amount of photons traveling from an emitter to a detector, the corresponding fMRI signal to the NIRS signal can be related to the average BOLD signal in all voxels along the photon-traveling pathway. However, because the exact shape of the pathway was unknown, we used a spherical region underneath each channel marker (vitamin tablets attached on a probe holder, see Fig. 2B) as an approximation of an ROI, which was determined using the following processes with the anatomical image of each participant before normalizing the MNI space. First, the spherical region around the projection point of each channel was determined, which showed the radius of the sphere was 7.5 mm. Second, by removing any portion of the sphere that fell outside the gray matter mask and keeping only the voxels inside the gray matter, we determined 14 ROIs in the structural image of each participant (Fig. 3C). Subsequently, by normalizing these ROIs to the MNI space and identifying commonly included voxels between these ROIs and the functional volumes (Fig. 1, "NIRS-ROI mask normalization"), we extracted and averaged fMRI signals inside these voxels (Fig. 1, "Seed signal extraction from NIRS-ROI"). Thus, for each NIRS time-course, we obtained a corresponding BOLD time-course. The anatomical name of each ROI was determined in the MNI space by referring to the anatomical

Table 1

Locations of predefined ROIs of 3 resting state networks.

Network	Name of ROI used in the previous study	Corresponding name in the AAL	MNI coordinates		
			x	y	z
Dorsal attention	IMT +	Occipital_Mid_L	-45	-69	-2
Fronto-parietal	raPFC	Frontal_Mid_R	34	52	10
Default	vmPFC	Frontal_Med_Orb_L	0	51	-7

All MNI coordinates have been reported in the previous studies (Fox et al., 2005; Vincent et al., 2008). Abbreviations: r/R = right, l/L = left, MT+ = middle temporal area, aPFC = anterior prefrontal cortex, vmPFC = ventromedial prefrontal cortex, Mid = middle, Med = medial part, Orb = orbital part.

location of the centroid that was calculated as the centroid of all centroids of the ROIs estimated in individual data sets.

3. BOLD time-series used to produce each predefined RSN: Seed regions of BOLD time-series used to estimate the predefined RSNs were extracted from ROIs in the MNI space (Fig. 1, "Seed signal extraction from predefined ROI"). The MNI coordinates reported by previous reports (Fox et al., 2005; Vincent et al., 2008; Table 1) were used to define the dorsal attention, the fronto-parietal control, and the default mode networks.

By calculating the cross-correlation at lag 0 between the BOLD time-series of voxels from the whole brain and the above-mentioned seed time-series, we obtained 3 types of correlation maps (maps calculated with NIRS signals [oxy-map and deoxy-map], corresponding BOLD signals [cBOLD-map], and RSNs [DA-map, FPC-map, and DM-map]) for each participant's data (Fig. 1, "Seed-based correction maps calculation"). All maps were processed using Fisher's Z transformation. Subsequently, a Student's *t*-statistic map (random effects analysis; uncorrected) was computed for each data set (Fig. 1, "Population-based Z-score maps calculation"). Because distributions of *p*-values were different between maps calculated with seed signals acquired with different devices, we thresholded each map based on the distribution of *p*-values.

Similarity of correlation maps

To evaluate the similarity of spatial distribution between the oxy-map, deoxy-map, and cBOLD-map for each measurement channel, we computed the standard Pearson correlation coefficient over all gray matter voxels within the cerebral cortex in each participant (Fox et al., 2006; Vincent et al., 2007; Fig. 1, "Spatial correlation between correlation maps"). Statistical significance was tested using a two-

Table 2

Locations of gravity points of normalized ROIs corresponding to NIRS channels.

Number of channel	Anatomical location of gravity point	MNI coordinates			SD
		Position			
		x	y	z	
1	Frontal_Sup_Medial_L	-1.9	59.3	5.4	8.4
2	Frontal_Sup_R	20.1	64.5	5.4	5.9
3	Frontal_Sup_L	-24.5	61.3	4.1	5.8
4	Frontal_Mid_R	40.6	53.2	2.4	6.9
5	Frontal_Mid_Orb_L	-43.4	47.4	-6.9	5.4
6	Frontal_Inf_Tri_R	51.4	32.7	1.2	7.4
7	Frontal_Inf_Orb_L	-47.9	23.7	-14.2	9.3
8	Temporal_Mid_R	54.0	-64.0	-0.5	10.4
9	Temporal_Mid_L	-56.1	-62.2	6.7	10.0
10	Occipital_Mid_R	41.2	-81.5	5.5	10.2
11	Occipital_Mid_Ant_L	-43.4	-82.0	9.1	10.5
12	Occipital_Sup_R	20.3	-94.9	6.2	12.6
13	Occipital_Mid_Post_L	-24.5	-95.1	9.8	11.2
14	Calcarine_L	-3.0	-93.6	8.8	12.2

The most likely anatomical labels are shown. Anatomical labels were determined by using the Automated Anatomical Labeling (AAL) (Tzourio-Mazoyer et al., 2002). All values are in millimeters. 'SD' stands for standard deviation. Abbreviations: L = Left hemisphere, R = Right hemisphere, Sup = Superior, Mid = Middle, Inf = Inferior, Ant = Anterior, Post = posterior, Orb = Orbital part, Tri = Triangular part.

Table 3

Proportion of centroids of ROIs across participants.

Ch	1st	%	2nd	%	3rd	%	4th	%
1	Frontal_Sup_Medial_L	70.4	Frontal_Sup_Medial_R	14.8	Frontal_Med_Orb_R	7.4	Cingulum_Ant_L	7.4
2	Frontal_Sup_R	92.3	Frontal_Sup_Orb_R	3.8	Frontal_Sup_Medial_R	3.8		
3	Frontal_Sup_L	74.1	Frontal_Mid_L	14.8	Frontal_Sup_Orb_L	11.1		
4	Frontal_Mid_R	75.0	Frontal_Mid_Orb_R	21.4	Frontal_Inf_Tri_R	3.6		
5	Frontal_Mid_Orb_L	60.7	Frontal_Inf_Orb_L	28.6	Frontal_Inf_Tri_L	7.1	Frontal_Mid_L	3.6
6	Frontal_Inf_Tri_R	82.1	Frontal_Inf_Orb_R	17.9				
7	Temporal_Pole_Sup_L	55.6	Frontal_Inf_Orb_L	40.7	Frontal_Inf_Tri_L	3.7		
8	Temporal_Mid_R	57.1	Temporal_Inf_R	39.3	Occipital_Mid_R	3.6		
9	Temporal_Mid_L	82.1	Occipital_Inf_L	7.1	Angular_L	7.1	Temporal_Inf_L	3.6
10	Occipital_Mid_R	78.6	Occipital_Inf_R	21.4				
11	Occipital_Mid_L	85.7	Occipital_Inf_L	10.7	Temporal_Mid_L	3.6		
12	Occipital_Sup_R	44.0	Calcarine_R	20.0	Cuneus_R	16.0	Occipital_Mid_R	12.0
13	Occipital_Mid_L	78.6	Occipital_Sup_L	10.7	Occipital_Inf_L	10.7		
14	Calcarine_L	48.0	Cuneus_L	44.0	Occipital_Sup_L	4.0	Lingual_L	4.0

The four most likely anatomical labels are shown. Anatomical labels were determined by using the Automated Anatomical Labeling (AAL) (Tzourio-Mazoyer et al., 2002). Abbreviations: L = Left hemisphere, R = Right hemisphere, Sup = Superior, Mid = Middle, Med = medial part, Inf = Inferior, Ant = Anterior, Post = posterior, Orb = Orbital part, Tri = Triangular part.

tailed *t*-test over subjects (random effects analysis) against the null hypothesis of no spatial correlation. The FDR method was used to correct for multiple comparisons, and significant connections were defined at $p < 0.05$ after FDR correction (Benjamini and Yekutieli, 2001).

It is likely that NIRS signals measured within the cortical region of RSNs include the information characterizing the spatial distribution of correlation coefficients in those RSN maps. To investigate this hypothesis, we also quantitatively compared spatial correlation between the maps and performed *t*-tests against 0, considering the individual data as random effects. To correct for multiple comparisons and significant connections, FDR correction was adopted.

Results

Registration of NIRS channels in the structural MRI

The anatomical locations of NIRS channels are summarized in Table 2. The mean MNI coordinates of centroids across all participants

are shown for each NIRS channel. The standard deviation of centroids of each NIRS channel represents the positional variations of centroids across the participants. The mean of the standard deviations across all channels was 9 mm. Each channel was anatomically labeled by applying AAL to the averaged MNI coordinates. All but 2 channels were located in different regions defined by AAL, whereas channels 11 and 13 were located within the same region (Occipital_Mid_L). Therefore, we renamed these 2 channels as Occipital_Mid_Ant_L and Occipital_Mid_Post_L, respectively. Generally, the centroids of a channel across all participants were not consistently located within the same brain region in the AAL system, due to the spatial variability across the participants. The 4 most likely anatomical locations of each channel are shown in Table 3.

Evaluation of regions where hemodynamic fluctuations are detected as NIRS signals obtained during the resting state

The representative examples of both resampled oxy-Hb and deoxy-Hb signals are shown in Fig. 4. The descriptive statistics of

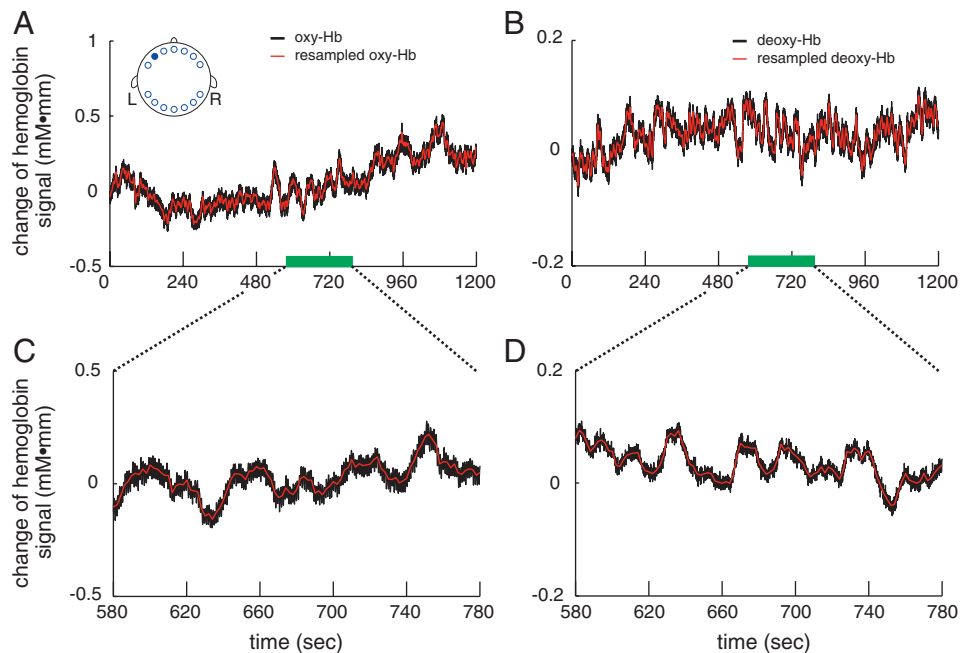


Fig. 4. Representative examples of continuous data for one participant. The channel of interest is shown in (A). (A) Oxy-Hb time-courses (black) and resampled data (red). The green bar indicates the enlarged section. (B) Deoxy-Hb time-courses (black) and resampled data (red). (C) Enlarged section of original oxy-Hb (black) and resampled data (red). (D) Enlarged section of deoxy-Hb (black) and resampled data (red).

Table 4
Descriptive statistics of LBCV.

Ch	Anatomical location of channel	oxy-Hb averaged distance	SD	Averaged r value	deoxy-Hb averaged distance	SD	Averaged r value
1	Frontal_Sup_Medial_L	4.6	1.8	0.39	5.4	1.7	-0.37
2	Frontal_Sup_R	5.2	1.7	0.49	5.4	1.7	-0.46
3	Frontal_Sup_L	5.8	2.3	0.48	5.1	2.0	-0.49
4	Frontal_Mid_R	4.9	1.9	0.42	6.0	2.4	-0.43
5	Frontal_Mid_Orb_L	5.2	1.5	0.33	5.7	1.9	-0.39
6	Frontal_Inf_Tri_R	5.4	1.8	0.29	5.8	1.5	-0.29
7	Frontal_Inf_Orb_L	5.0	1.4	0.26	5.6	1.7	-0.28
8	Temporal_Mid_R	4.9	2.3	0.47	5.4	2.0	-0.41
9	Temporal_Mid_L	5.2	1.8	0.43	5.2	2.1	-0.38
10	Occipital_Mid_R	5.3	1.8	0.52	5.3	1.6	-0.46
11	Occipital_Mid_Ant_L	6.6	2.0	0.45	5.4	1.8	-0.38
12	Occipital_Sup_R	6.3	1.6	0.55	6.4	1.7	-0.52
13	Occipital_Mid_Post_L	5.4	1.9	0.55	6.0	2.3	-0.50
14	Calcarine_L	5.0	1.7	0.51	5.4	1.5	-0.38

Anatomical labels were determined by using the Automated Anatomical Labeling (AAL) (Tzourio-Mazoyer et al., 2002). Values in the columns indicated as 'averaged distance' and 'SD' are in millimeters, while those in the columns indicated as 'averaged r value' are correlation coefficients. 'averaged distance', 'SD' and 'averaged r value' stands for averaged distance of the LBCV from the projection point across all participants, standard deviation and averaged correlation coefficients of the LBCV across all participants. Abbreviations: L = Left hemisphere, R = Right hemisphere, Sup = Superior, Mid = Middle, Inf = Inferior, Ant = Anterior, Post = posterior, Orb = Orbital part, Tri = Triangular part.

LBCVs are shown in Table 4. Based on these data, the average distance across all channels was 5.3 mm for oxy-Hb and 5.6 mm for deoxy-Hb, whereas the standard deviation was 0.6 and 0.4, respectively. This result demonstrates that most of the LBCVs were located within the radius of 2 voxels from the projection point. Although most of the averaged correlation coefficients were higher than 0.3 for oxy-Hb and lower than -0.3 for deoxy-Hb, the absolute values in Frontal_Inf_Tri_R and Frontal_Inf_Orb_L were slightly lower than those in the other brain regions (Table 4).

To investigate the distribution of regions where hemodynamic changes affect the obtained NIRS signals at the brain tissue level, we sorted HCVs (top 100 ranked voxels within a 3-cm radius from the projection point) by the tissue type. Most of the HCVs with both Hb signals were located within the brain tissue, whereas the HCVs in 2 brain regions (Frontal_Inf_Tri_R, Frontal_Inf_Orb_L) were located equally in the brain and non-brain tissues (Table 5). By picking up more than 100 voxels as HCVs and sorting by tissue types, the robustness of the result shown in Table 5 was confirmed (Table S1). These results show that NIRS signals obtained with all but 2 channels

Table 5
Distributions of HCVs with NIRS signals.

Ch	Anatomical location of channel	oxy-Hb brain tissue (%)	Skull (%)	Skin (%)	r value of 100th ranked voxel	deoxy-Hb brain tissue (%)	Skull (%)	Skin (%)	r value of 100th ranked voxel
1	Frontal_Sup_Medial_L	92	6	2	0.33	89	8	3	-0.30
2	Frontal_Sup_R	95	3	2	0.41	93	4	3	-0.37
3	Frontal_Sup_L	93	4	3	0.40	94	4	2	-0.40
4	Frontal_Mid_R	85	5	10	0.32	81	7	12	-0.31
5	Frontal_Mid_Orb_L	70	9	21	0.29	72	8	20	-0.32
6	Frontal_Inf_Tri_R	51	10	39	0.25	55	10	35	-0.24
7	Frontal_Inf_Orb_L	37	9	54	0.25	51	8	41	-0.26
8	Temporal_Mid_R	94	3	3	0.41	90	5	5	-0.34
9	Temporal_Mid_L	91	5	4	0.36	85	7	8	-0.31
10	Occipital_Mid_R	95	2	3	0.49	88	5	7	-0.41
11	Occipital_Mid_Ant_L	94	4	2	0.45	85	8	7	-0.36
12	Occipital_Sup_R	96	2	2	0.54	88	6	6	-0.47
13	Occipital_Mid_Post_L	94	4	2	0.50	89	6	5	-0.44
14	Calcarine_L	92	5	3	0.46	81	10	9	-0.35

Anatomical labels were determined by using the Automated Anatomical Labeling (AAL) (Tzourio-Mazoyer et al., 2002). Values in the columns indicated as 'r value of 100th-ranked voxels' are correlation coefficients. 'r value of 100th-ranked voxels' stands for averaged 100th-ranked correlation coefficients of the HCVs across all participants. Abbreviations: L = Left hemisphere, R = Right hemisphere, Sup = Superior, Mid = Middle, Inf = Inferior, Ant = Anterior, Post = posterior, Orb = Orbital part, Tri = Triangular part.

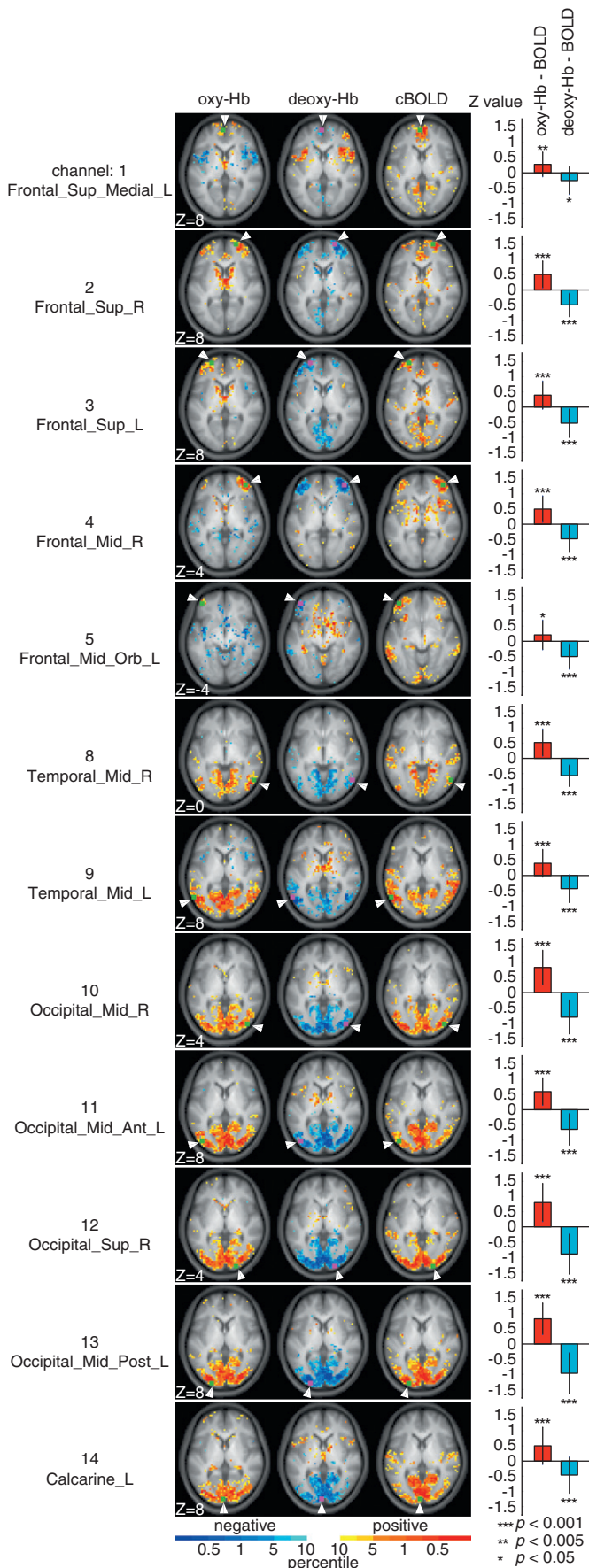
mainly reflect changes in the Hb concentration that occur in the brain regions adjacent to the channels during the resting state.

Whole brain distribution of correlated voxels with NIRS signals obtained during the resting state

To calculate group-averaged statistical maps of cross-correlation, we used oxy-Hb signals, deoxy-Hb signals, and BOLD signals extracted from the ROIs corresponding to the NIRS measurement regions as seed signals (Fig. 5). Because of the inconsistency between participants in the tissue type where hemodynamics were reflected in NIRS signals, we did not use signals from Frontal_Inf_Tri_R (channel 6) or Frontal_Inf_Orb_L (channel 7) for calculating the map. For each channel, oxy-maps and cBOLD-maps provided closely resembling spatial distributions, whereas deoxy-maps were clearly similar to the inversed patterns of both oxy-maps and cBOLD-maps. Spatial correlation analyses demonstrated that the oxy-maps and cBOLD-maps had a significant positive correlation for all brain regions (Fig. 5, bar graphs). Significant negative correlation was observed between deoxy-maps and cBOLD-maps for all brain regions. These results demonstrate that using NIRS signals measured at various brain regions as seed signals can reproduce the specific distribution patterns of correlation maps generated using BOLD signals extracted from the corresponding seed brain regions.

To identify the non-brain tissue regions that correlated with NIRS signals obtained at Frontal_Inf_Tri_R and Frontal_Inf_Orb_L, we examined the correlation maps using NIRS signals obtained in these regions as seed signals in individual data. We focused examination on 2 participants whose data showed that over half of all correlating voxels with NIRS signals obtained in these 2 regions were located within the non-brain tissue regions. The correlation map estimated for each individual's data is shown in Supplemental Figure S1. We found that the correlating voxels mainly localized not within the brain regions but rather within the bilateral temporal muscles and/or in the tissues near the eyes. Furthermore, an overlap was observed between most of the voxels correlating with the NIRS signal obtained at the Frontal_Inf_Tri_R and the Frontal_Inf_Orb_L.

The effect of noise regression in BOLD signals on the correlation between NIRS and BOLD signals was examined (Fig. S2). When no waveform was regressed from the BOLD signals, both the Hb signals correlated not only with the cortical regions but also with cerebral vasculatures such as the superior sagittal sinus and the transverse sinus. Conversely, when all physiological waveforms (see "Noise signal regression" in the Materials and methods section) were regressed from the BOLD signals, no correlation over threshold was observed in these cerebral vasculature areas.



We also calculated group-averaged statistical maps with BOLD signals extracted from predefined ROIs (DA-map, FPC-map, and DM-map) so that we could determine whether NIRS signals obtained in these areas were correlated with the specific brain regions of these RSNs. The nearest NIRS channels from the predefined ROIs of the dorsal attention and fronto-parietal control networks were located within the same anatomical regions as these ROIs (Occipital_Mid_Ant_L and Frontal_Mid_R), whereas the nearest channel to the ROI of the default mode network was located in the next regions, based on AAL (NIRS channel: Frontal_Sup_Medial_L, ROI: Frontal_Med_Orb_L). The regions positively correlated with oxy-Hb signals and negatively correlated with deoxy-Hb signals in the Occipital_Mid_Ant_L region were mainly localized within the bilateral inferior temporal gyri, bilateral lingual gyri, right inferior precentral gyrus, and bilateral superior parietal lobule. These brain regions correspond to the regions that have been repeatedly reported as the “dorsal attention network.” The DA-map calculated using BOLD signals extracted from the left MT+ region, which corresponds to the Occipital_Mid_L in the AAL, as seed signals also showed positive correlation in these regions (Figs. 6A, B). The regions positively correlated with oxy-Hb signals and negatively correlated with deoxy-Hb signals in the Frontal_Mid_R were mainly localized within the bilateral dorsolateral prefrontal cortices, right dorsomedial prefrontal cortex/anterior cingulate, and right anterior inferior parietal lobule. These brain regions correspond to the regions that have been repeatedly reported as the “fronto-parietal control network.” The FPC-map calculated using BOLD signals extracted from the right aPFC region, corresponding to the Frontal_Mid_R in the AAL, as seed signals also showed positive correlation in these regions (Figs. 6C, D). The regions positively correlated with oxy-Hb signals and negatively correlated with deoxy-Hb signals in the Frontal_Sup_Medial_L were mainly localized within the ventromedial prefrontal cortex, bilateral lateral parietal cortices, bilateral superior frontal cortices, and posterior cingulate. These brain regions correspond to the regions also known as the “default mode network.” The DM-map calculated using BOLD signals extracted from right vmPFC, corresponding to the Frontal_Med_Orb_L in the AAL, as seed signals also showed positive correlation in these regions (Figs. 6E, F). Spatial correlation analysis revealed that the spatial distributions of correlation coefficients in the oxy-maps and deoxy-maps calculated with signals obtained from the Occipital_Mid_Ant_L, Frontal_Mid_R, and Frontal_Sup_Medial_L were correlated positively and negatively, respectively, with those of the DA-map, FPC-map, and DM-map (Figs. 6G–I). These results demonstrate that NIRS signals obtained at the brain regions of dorsal attention, fronto-parietal control, and default mode networks correlated with spontaneous hemodynamic fluctuation determining the spatial patterns of those RSNs.

A previous study demonstrated that the regions within the fronto-parietal control network are spatially interposed between regions within the dorsal attention and default mode networks, especially

Fig. 5. Group-average statistical maps of correlation corresponding to varied seed locations and different NIRS seed signals. Each row corresponds to the location of the seed represented by NIRS measurement channels and their projected locations on the cortex. The left, middle, and right maps in each row represent those calculated using different seed signals: oxy-Hb signal, deoxy-Hb signal, and BOLD signal extracted from the ROI around the projection point (Fig. 3), respectively. The voxels with upper 10% of p -value are colored. The dots indicated by arrowheads (green dots in the left and right maps and pink dots in the middle map) show the cortical projection point of the vitamin tablet representing the NIRS measurement channel. The red and blue bar graphs on the right side of the images represent the spatial correlations between the maps calculated using oxy-Hb signals as seed signals and that calculated with seed BOLD signals, and those between the maps calculated using deoxy-Hb signals as seed signals and that calculated with seed BOLD signals, respectively. The error bars indicate standard deviations. Significant spatial correlation coefficients against 0 are shown (* $p < 0.05$, ** $p < 0.01$, *** $p < 0.001$).

within the parietal cortex (Vincent et al., 2008). To determine whether NIRS signals obtained in brain regions near these 3 RSNs could characterize this spatial relation among the RSNs, we investigated the distributions of the superficial cortical regions correlated with NIRS signals obtained from the Occipital_Mid_Ant_L, Frontal_Mid_R, and Frontal_Sup_Medial_L. We found that there was very little overlap of regions positively correlated with oxy-Hb signals and negatively correlated with deoxy-Hb signals obtained for these 3 regions (Figs. 7A, B). In particular, regions positively correlated with oxy-Hb signals and negatively correlated with deoxy-Hb signals in the Frontal_Mid_R and Frontal_Sup_Medial_L were anteroposteriorly separately localized within the inferior parietal regions (Parietal_Inf_R, SupraMarginal_R, Parietal_Inf_L, and SupraMarginal_L for Frontal_Mid_R; Angular_R and Angular_L for Frontal_Sup_Medial_L), whereas those positively correlated with oxy-Hb signals and negatively correlated with deoxy-Hb signals in the Occipital_Mid_Ant_L were localized in more superior cortical regions (Parietal_Sup_R and Parietal_Sup_L). For each channel, non-overlapping voxels were more than 89% of all voxels positively correlated with oxy-Hb signals of the channel, and were more than 93% of all voxels negatively correlated with deoxy-Hb signals of the channel. These results demonstrate that NIRS signals obtained within brain regions of these RSNs estimated in previous fMRI studies include adequate information to localize those RSNs within plausibly separate anatomical regions. By comparing the spatial patterns of the DA-map, FPC-map, and DM-map in superficial brain regions, we confirmed this positional relationship between these 3 networks within the fMRI data set (Fig. 7C).

Discussion

The purpose of this study was to investigate and establish the relationship between NIRS and fMRI during the resting state to study functional connectivity with special focus on the RSNs. To do so, we conducted simultaneous recording of NIRS and fMRI and the following analyses. First, we identified the positions of NIRS channels in the cortical regions using individual data sets and investigated the distribution of these positions across participants in the MNI space. Second, we tried to find the local maximum of the correlation coefficient between NIRS and fMRI signals in the regions close to the NIRS channel. Third, we classified the highly correlated voxels with NIRS signals that resided in the adjacent regions to NIRS channels into brain and non-brain voxels. Finally, we investigated whether NIRS signals correlated with BOLD signals not only within the adjacent brain regions to NIRS channels but also within distant brain regions constituting RSNs. Accordingly, there are 4 corresponding findings in this study. First, we successfully projected all NIRS measurement channels onto the cortical surface with an average standard deviation of 9 mm (Table 2), which is similar to a previously reported value by Okamoto et al. (2004). Second, we found single voxels, which corresponded to the local maxima of correlation coefficients between NIRS and fMRI signals, within a radius of 2 voxels from the projection point independent of the channel location (Table 4). Third, we observed that highly correlated voxels with the NIRS signal were mainly localized within brain tissues for all NIRS channels, except for 2 bilateral inferior frontal channels (Frontal_Inf_Tri_R and Frontal_Inf_Orb_L) (Table 5). Finally, we observed cortical regions correlating with the NIRS signals not only within areas adjacent to the channels but also in areas distant from the channels (Fig. 5). In particular, we successfully reproduced the correlation maps of 3 RSNs (dorsal attention, fronto-parietal control, and default mode networks) using NIRS signals as seed signals (Figs. 6, 7). Collectively, these findings support the idea that NIRS signals obtained at several cortical regions during the resting state mainly reflect regional spontaneous hemodynamic fluctuations that originate from spontaneous cortical activity and include information characterizing cortico-cortical resting state functional connectivity.

Registration of NIRS channels in the structural MRI

In the current study, we assumed that obtained NIRS signals should mainly reflect hemodynamics of regions along the optical path plane, because it has previously been reported that the photon-traveling pathways have a “banana” shape between the incident and detection probes (Okada et al., 1997; van der Zee et al., 1990) (see *Materials and methods*). Therefore, we applied a different procedure for registration of NIRS channel positions on the cortical regions that the previous study that examined cranio-cerebral correlation using magnetic resonance imaging (MRI), via the guidance of the international 10–20 system for electrode placement (Okamoto et al., 2004). To confirm the reliability of the registration process, we examined whether changes in the projection point of the NIRS channel produced by rotation of the optical path plane affected the resultant correlation between NIRS signals (oxy-Hb and deoxy-Hb) and BOLD signals extracted from spherical ROIs around the projection point (see supplementary materials for detailed account of the procedure). The best correlation was found between NIRS signals and BOLD signals extracted from the ROI around the projection point without rotation (Fig. S3), indicating that the process can reliably register the channel location on the cortical surface. All channels were projected on the cortical surface with similar accuracy to that previously reported. Cui et al. (2011) projected the channel marker from the scalp to the brain surface by finding the point on the brain surface that was closest to the marker, which is similar to the procedure used by Okamoto et al. (2004). Furthermore, Cui et al. (2011) reported that the mean value of the distances between the LBCVs and projection points was 18 mm for oxy-Hb signals and 21 mm for deoxy-Hb signals. In the current study, we found the LBCVs were within a radius of 2 voxels (~6 mm) from the projection point, suggesting that the method of registration applied in our study is also useful in addition to those methods used in the aforementioned previous studies.

Regions where hemodynamic fluctuations were reflected by NIRS signals obtained during the resting state

The fact that LBCVs were found within a radius of 2 voxels from the projection point supports that both oxy-Hb and deoxy-Hb signals reflect hemodynamic fluctuations in regions adjacent to the measurement channels. Furthermore, highly correlated voxels with each of the Hb signals were found within brain tissues regardless of which of the Hb signal was used to calculate correlation (Table 5). Therefore, correlation between fMRI signals within cortical regions and NIRS signals reported in the current study mainly reflects coherence of hemodynamic changes due to spontaneous cortical activity. On the other hand, NIRS signals obtained at the 2 frontal regions (Frontal_Inf_Tri_R and Frontal_Inf_Orb_L) showed correlation not only with BOLD signals from brain tissues but also with those from non-brain tissues (Table 5). Among these signals, we found a strong correlation between the NIRS signals obtained at the 2 frontal channels (Frontal_Inf_Tri_R and Frontal_Inf_Orb_L) and the whole head BOLD signals in the soft tissue, such as bilateral temporal muscles and/or tissues near the eyes (Fig. S1). This finding indicates that NIRS signals obtained at these areas mainly reflect Hb concentration changes in the soft tissue, as shown in the lower proportions of brain tissues in the highly correlated voxels in Table 5. Also of note, Cui et al. (2011) demonstrated that the scalp-brain distance affects the NIRS–fMRI correlation. However, the distance between these 2 channels and brain surfaces did not have a strong effect on the results of the current study. Although it is unclear why NIRS signals in only 2 frontal regions showed correlation with those outside of the brain tissue, it is likely that signals in these regions are more strongly affected by global changes of Hb concentrations, such as skin blood flow, than the other regions (Gagnon et al., 2012a, 2012b; Kohno et al., 2007; Obrig et al., 2000; Saager and Berger, 2008; Tachtsidis et al., 2008; Takahashi et al., 2011; Toronov et al., 2001;

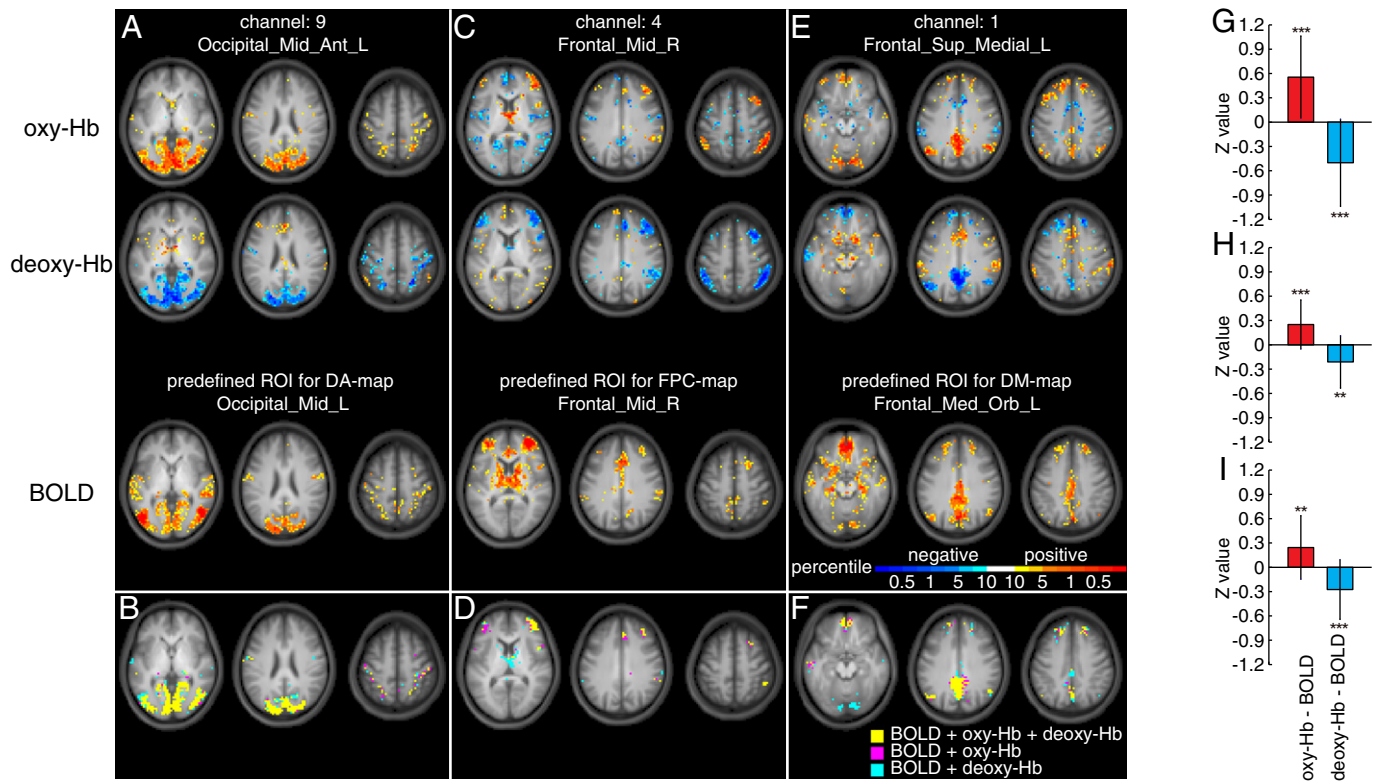


Fig. 6. RSNs revealed using NIRS signals and BOLD signals as seeds. Group-average statistical maps calculated using Hb signals and BOLD signals extracted from predefined ROIs as seed signals. The top and middle rows show oxy-maps and deoxy-maps calculated using Hb signals obtained at (A) Occipital_Mid_Ant_L, (C) Frontal_Mid_R, and (E) Frontal_Sup_Medial_L. The bottom row shows maps calculated using BOLD signals extracted from predefined ROIs (Table 1) located within (A) Occipital_Mid_L, (C) Frontal_Mid_R, and (E) Frontal_Med_Orb_L areas. BOLD signals extracted from these areas have been reported to correlate with brain regions of (A) dorsal attention, (C) fronto-parietal control, and (E) default mode networks. (B), (D) and (F) correspond to the conjunction maps of (A), (C), and (E), respectively. Yellow, magenta, and cyan regions were colored as brain regions correlating with BOLD signals and both Hb signals used as seed signals; with BOLD signals and oxy-Hb signals; and with BOLD signals and deoxy-Hb signals, respectively. In (A–F), we thresholded each map at the value of the top 10% of the distribution of p -values of all brain voxels, because the distributions of p -values were different between maps calculated with seed signals acquired with different devices. (G–I) Spatial correlation between the map calculated using Hb signals as seed signals and that calculated with BOLD signals. The error bars indicate standard deviations. The significant spatial correlation coefficients against 0 are shown (** $p < 0.01$, *** $p < 0.001$).

Yamada et al., 2009; Zhang et al., 2007). In particular, Gagnon et al. (2012b) showed that systemic interference occurring in the superficial layers of the human head is inhomogeneous across the surface of the scalp. To clarify the issue, it would be helpful to investigate the effect of the motion of the cephalic muscles and blood stanching on the NIRS signals obtained at these regions. In addition, the effect of the posture of participants during measurement on the results must be clarified. Although we measured NIRS signals with individuals in the face-up position, NIRS measurements are generally conducted with

participants sitting. Because this positional difference of the participants can affect their blood flow circulation, it would be useful for future studies to focus on the relevance of participant's posture to functional connectivity. Whatever the case, the present study demonstrated that NIRS can detect regional changes in cortical blood oxygenation during the resting state, though we must be very careful about taking measurements at some restricted head positions, such as the inferior frontal gyrus where changes in signals are dominated by those originated from non-brain tissues.

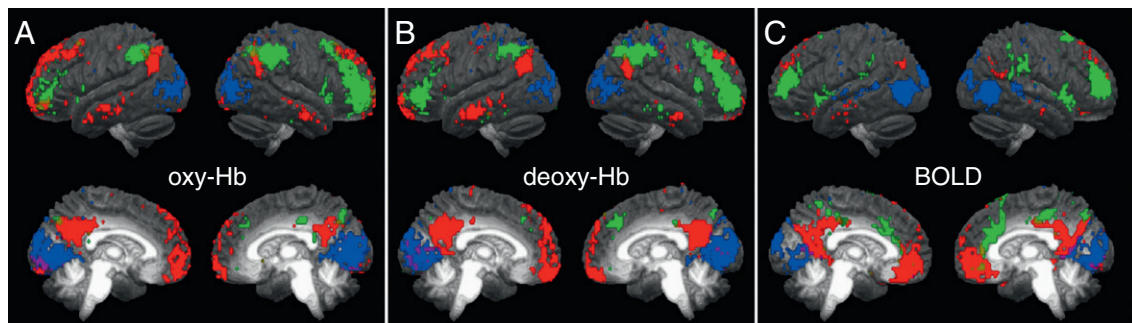


Fig. 7. Anatomical separation of RSNs. (A) Positively correlated regions with oxy-Hb seed signals. Blue, green, and red represents the voxels with p -values within the upper 5% of all cortical voxels that were positively correlated with oxy-Hb signals obtained at Occipital_Mid_Ant_L, Frontal_Mid_R, and Frontal_Sup_Medial_L, respectively. (B) Negatively correlated regions with deoxy-Hb seed signals. Blue, green, and red represents the voxels with p -values within the upper 5% of all cortical voxels that were negatively correlated with deoxy-Hb signals obtained at Occipital_Mid_Ant_L, Frontal_Mid_R, and Frontal_Sup_Medial_L, respectively. (C) Positively correlated regions with BOLD signals. Blue, green, and red represents the voxels with p -values within the upper 5% of all cortical voxels that were positively correlated with BOLD signals extracted from predefined ROIs (Table 1) at Occipital_Mid_L, Frontal_Mid_R, and Frontal_Med_Orb_L, respectively. In this figure, we defined cortical voxels as those classified into cortical regions with AAL.

Whole brain distribution of correlated voxels with NIRS signals obtained during the resting state

By calculating the cross-correlation, we observed that spatial patterns of correlating brain regions with NIRS signals were similar to those of correlating regions with BOLD signals extracted from areas close to NIRS channels (Fig. 5). RSNs have been reported in many fMRI studies using seed-based correlation analysis (Biswal et al., 1995; Damoiseaux et al., 2006; Fox et al., 2005; Fransson, 2005; Greicius et al., 2003; Vincent et al., 2008) and independent component analysis (Beckmann et al., 2005; Calhoun et al., 2001; De Luca et al., 2006; van de Ven et al., 2004). Despite the different methods used to characterize the RSNs, specific brain regions have been consistently reported as the RSNs across studies (van den Heuvel and Hulshoff, 2010). In the present study, we used NIRS and fMRI simultaneously to successfully reproduce 3 RSNs (dorsal attention, fronto-parietal control, and default mode networks), using NIRS signals instead of fMRI signals as seed signals (Beckmann et al., 2005; Damoiseaux et al., 2006; De Luca et al., 2006; Fox et al., 2005; Fransson, 2005; Greicius et al., 2003; van den Heuvel et al., 2008; Vincent et al., 2008) (Fig. 6). It should be noted that the voxels that did not satisfy the significance level ($p < 0.05$, corrected) could be included in the correlation maps thresholded with our method. However, considering that the spatial patterns of previously reported RSNs could be successfully reproduced using both NIRS and BOLD signals, our results strongly support the theory that both oxy-Hb and deoxy-Hb signals can detect the information necessary for determining RSNs included in the fMRI data sets. On the other hand, the BOLD response theoretically results from local concentration changes in paramagnetic deoxy-Hb (Ogawa et al., 1990). Previous studies on functional activation revealed a strong temporal and spatial correlation of the BOLD signal with deoxy-Hb, rather than oxy-Hb (Huppert et al., 2006a, 2006b). In contrast, the current study showed that both oxy-Hb and deoxy-Hb produced consistent results in terms of the spatial patterns of the correlation maps. Although the relationships between each of the Hb signals and the BOLD signals are not fully understood (Chen et al., 2011; Devor et al., 2007; Steinbrink et al., 2006), our results suggest that resting state functional connectivity may arise at least in part from the coupling of spontaneous neural activity that is commonly reflected in cerebral hemodynamic changes in different blood vessels such as arterioles, capillaries, and venules.

Conversely, a previous study indicated that the low-frequency components (0.01–0.1 Hz) of NIRS signals obtained during the resting state were affected by fluctuations in the blood flow and hemoglobin oxygenation at a global circulatory system level (Tong and Frederick, 2010). In this previous study, the authors showed that the spatiotemporal patterns of regions correlating with NIRS signals obtained at the right prefrontal area resembled the spatial patterns of the cerebral venous system. In the current study, when the preprocessing step of the fMRI data similar to the one used in the previous study was adopted, we also observed a correlation over threshold within the cerebral venous regions (Fig. S2). This finding suggests that both NIRS and BOLD signals may include the correlating information of physiological noises originating from non-brain tissue even after being processed with the band-pass filter (0.009–0.1 Hz). However, the correlation within vasculature areas was not found in the correlation maps calculated with the current preprocessing step, which fully regresses out the noises in fMRI data. Furthermore, some RSNs can be successfully reproduced using NIRS instead of fMRI signals as seed signals (Figs. 5, 6). This result supports the theory that, although NIRS signals obtained during the resting state may be contaminated with physiological noises, they evidently also contain information representing the spontaneous cortical activity that characterizes RSNs.

Recently, another study showed that simultaneously measured NIRS and fMRI signals produce similar resting state functional connectivity between the bilateral primary motor areas (Duan et al.,

2012). In that study, the authors transformed the fMRI data into the NIRS measurement space and estimated the functional connectivity in that space. Generally, NIRS-based functional connectivity is estimated by calculating the cross-correlation of signals obtained from different channels. In our previous NIRS study, we calculated the cross-correlation between all pairs of NIRS signals obtained from diverse brain regions and observed the functional connectivity between bilateral homologous brain regions (Sasai et al., 2011). This finding was reproduced using the same analysis with the NIRS signals measured in the current study (data not shown). Thus, accumulated evidence shows that NIRS-based functional connectivity is consistent with fMRI-based functional connectivity.

The dorsal attention and default mode networks have been suggested to have competing functions, that is, information processing from the external world versus internal mentation (Buckner and Vincent, 2007; Buckner et al., 2008; Corbetta and Shulman, 2002; Gusnard et al., 2001; Mason et al., 2007). Recent fMRI studies focused on switching between these RSNs (depending on the experimental conditions) demonstrated that the interaction of the dorsal attention and default mode networks is causally regulated by the fronto-parietal control network (Gao and Lin, 2012; Sridharan et al., 2008). The fronto-parietal control network is anatomically interposed between the dorsal attention and default mode networks (Vincent et al., 2008). The results of the current study successfully reproduced the same anatomical relationship among these RSNs using NIRS (Fig. 6), which supports that use of NIRS can detect the cortical activity correlated only within the anatomically specific regions of these RSNs. This suggests that we can evaluate the relationship of these RSNs using NIRS signals obtained at cortical regions of these RSNs. Although we must establish the method to extract only the information determining RSNs from raw NIRS signals, the findings of our study promote the application of NIRS to prove the signal relationship among these RSNs.

Regarding the temporal relationship among the RSNs, many fMRI studies have reported a negative correlation between the dorsal attention and default mode networks (Fox et al., 2005, 2009; Fransson, 2005; Greicius et al., 2003; Kelly et al., 2008). To accurately estimate functional connectivity, a general linear model (GLM) technique has previously been used to remove fluctuations due to scanner instabilities, subject motion and respiration and cardiac effects, and the coherent signal fluctuations across the brain (global signal) (Fox et al., 2005, 2009). However, the regression of the global signal has also been shown to introduce spurious anti-correlated RSNs (Anderson et al., 2011; Murphy et al., 2009). Thus, it is still unclear whether anti-correlation between RSNs observed in fMRI studies reflects the negatively correlating patterns of spontaneous brain activity. On the other hand, although NIRS measurement was conducted on the diverse cortical regions, we could not find negative correlation among any pairs of NIRS channels in our previous NIRS study (Sasai et al., 2011) and the current study (data not shown). Although the results of the current study indicated that the signals acquired using both NIRS and fMRI represent the spontaneous neural activity characterizing RSNs, the attributes of noises included in these signals might be different. Considering this difference between fMRI and NIRS and the higher temporal resolution of NIRS, NIRS provides additional information on the temporal relationship between these RSNs. This finding supports the theory that NIRS is a valuable tool that can be used to measure the signals characterizing RSNs and to investigate the intrinsic dynamics of the human brain.

Issues for future studies

Recent studies have demonstrated the relationship between resting state networks and cognitive function and dysfunction. For example, the default mode network is suggested to take the central role in internally focused cognitive processes, such as mind

wandering (Christoff et al., 2009; Mason et al., 2007), self-reference (D'Argembeau et al., 2005; Gusnard et al., 2001), and recollecting one's past or imagining one's personal future (Schacter et al., 2007; Spreng et al., 2009), whereas the increased and decreased connectivity within the default mode network has been demonstrated to be linked to diverse psychiatric brain disorders (Fox and Greicius, 2010). Use of NIRS enables us to obtain the information on focused resting state networks easier than using fMRI, because the network information can be measured only by setting NIRS channels onto the regions related to targeting resting state networks. Although several challenges remain before the abnormality of the resting state networks can be used as a diagnostic marker in psychiatric disorders (Fornito and Bullmore, 2010; Fox and Greicius, 2010), the findings of the current study motivate clinical applications of NIRS to study resting state functional connectivity.

In the emerging social cognitive neuroscience literature, it has been suggested that some RSNs have functional roles in social cognition. For example, it has been reported that the activity of the default mode network is associated with the process of social cognition, such as mentalizing or reflecting on the mental states of others (Amodio and Frith, 2006; Buckner and Carroll, 2007; Gallagher and Frith, 2003; Mitchell et al., 2002; Mitchell et al., 2006; Rilling et al., 2004, 2008), and self-referential processing (D'Argembeau et al., 2005; Gusnard et al., 2001). Furthermore, both an activation in part of the fronto-parietal control network and a deactivation in the default mode network have been observed when participants were imitated, compared with when they imitated others (Guionnet et al., 2012). However, there are only a handful of studies that explore neural mechanisms of social interaction in an interactive context (Guionnet et al., 2012; Redcay et al., 2010; Saito et al., 2010; Schilbach et al., 2010; Tognoli et al., 2007), though social interaction is a coregulated coupling activity that involves at least two autonomous agents. As Guionnet et al. has pointed out, the major reason for this paucity may be attributed to the methodological and technical difficulties associated with creating a natural social interaction within an MRI environment. Considering that participants can have a direct face-to-face interaction while undergoing NIRS measurement, usage of NIRS makes it easier to measure the activity of the RSNs during social interaction (Cui et al., 2012; Funane et al., 2011). Therefore, our finding should promote investigation of the role of RSNs in social interaction.

In most fMRI and NIRS studies, functional connectivity has been explored by employing methods that assume temporal stationarity, such as cross-correlation. Using fMRI and NIRS independently, it has been previously investigated whether resting state functional connectivity estimated using signals obtained from these imaging techniques is test-retest reliable (Zhang et al., 2011 for NIRS; Zuo et al., 2010 for fMRI). On the other hand, recent fMRI studies have demonstrated that resting state functional connectivity exhibits dynamic changes within time scales of seconds to minutes (Chang and Glover, 2010; Kang et al., 2011). Furthermore, one study demonstrated that functional brain networks exhibit task-induced changes in their network topology (Moussa et al., 2011). Moreover, studies using electroencephalography demonstrated that cortical activation induced with transcranial magnetic stimulation during non-rapid eye movement sleep did not propagate other cortical areas, whereas waves of activation during quiet wakefulness moved to connected cortical areas several centimeters away (Massimini et al., 2005). This suggests that network topology of the RSNs also changes during the sleep state transitions. Because dynamic properties of a network relate to unfolding processes in the network (Butts, 2009), an understanding of the dynamic characteristics of a resting state network is important to reveal the intrinsic information on the processing mechanism of the brain, such as information exchange between different brain regions. Because NIRS requires less physical burden to participants, this device is useful for examining the characteristics of functional connectivity with a relatively long time-scale. Indeed,

one published NIRS study conducted long-term recording for over 1 hour at bedside (Roche-Labarbe et al., 2008). Thus, the results of our study should promote investigation of the dynamic characteristics of resting state functional connectivity.

NIRS should also be helpful for investigation of some other issues. Some studies have investigated changes in the RSNs along the course of development by measuring spontaneous brain activity of infants with fMRI and NIRS (Doria et al., 2010; Gao et al., 2009; Homae et al., 2010). However, it is often difficult to transport early preterm infants to an fMRI scanner, therefore there is limited data related to the RSNs in these periods (White et al., 2012). Because NIRS is suitable for use in conditions where participants have difficulty entering an fMRI scanner, application of NIRS should promote gathering of information on the RSNs from these participants. Furthermore, in previous fMRI studies, RSNs have generally been characterized from brain activity recorded with participants lying in the dorsal position inside the scanner. In contrast, NIRS measurement can be conducted without relation to the posture of the involved participant. Therefore, the effect of this postural difference on the RSNs can be investigated using NIRS by running resting state recording with participants in these 2 postures.

Conclusions

In this study, we evaluated the NIRS–fMRI signal relationship during the resting state, with particular emphasis on functional connectivity, by concurrently using fMRI and NIRS. Our results showed that NIRS can be used to collect information regarding RSNs defined in fMRI. This study should encourage development of signal analysis for elucidating the RSNs from measured NIRS signals.

Acknowledgments

We thank K. Asakawa for providing administrative assistance. We are grateful to M. Kato for providing assistance in experiments. We acknowledge T. Ishizuka and M. Fujiwara for providing technical assistance. This work was partly supported by Grants-in-Aid for the Japan Society for the Promotion of Science (JSPS) Fellows 2311065 (to S.S.), for Young Scientists (S) 20670001 (to G.T.), and for Challenging Exploratory Research 23650224 (to H.C.T.). In addition, it was partly supported by the Ministry of Education, Culture, Sports, Science and Technology in Japan (MEXT) for Scientific Research (S) 21220005 (to N.S.), and Scientific Research on Innovative Areas 22101007 (to H.C.T.). A part of this study is the result of “Development of biomarker candidates for social behavior” carried out under the Strategic Research Program for Brain Science by MEXT.

Appendix A. Supplementary data

Supplementary data to this article can be found online at <http://dx.doi.org/10.1016/j.neuroimage.2012.06.011>.

References

- Amodio, D.M., Frith, C.D., 2006. Meeting of minds: the medial frontal cortex and social cognition. *Nat. Rev. Neurosci.* 7, 268–277.
- Anderson, J.S., Druzgal, T.J., Lopez-Larson, M., Jeoung, E., Desai, K., Yurgelun-Todd, D., 2011. Network anticorrelations, global regression, and phase-shifted soft tissue correction. *Hum. Brain Mapp.* 32, 9–934.
- Ashburner, J., 2007. A fast diffeomorphic image registration algorithm. *NeuroImage* 38, 95–113.
- Beckmann, C.F., DeLuca, M., Devlin, J.T., Smith, S.M., 2005. Investigations into resting-state connectivity using independent component analysis. *Philos. Trans. R. Soc. Lond. B. Biol. Sci.* 360, 1001–1013.
- Benjamini, Y., Yekutieli, D., 2001. The control of the false discovery rate in multiple testing under dependency. *Ann. Stat.* 29, 1165–1188.
- Biswal, B., Yetkin, F.Z., Haughton, V.M., Hyde, J.S., 1995. Functional connectivity in the motor cortex of resting human brain using echo-planar MRI. *Magn. Reson. Med.* 34, 537–541.

- Buckner, R.L., Carroll, D.C., 2007. Self-projection and the brain. *Trends Cogn. Sci.* 11, 49–57.
- Buckner, R.L., Vincent, J.L., 2007. Unrest at rest: default activity and spontaneous network correlations. *NeuroImage* 37, 1091–1096 (discussion 1097–1099).
- Buckner, R., Andrews-Hanna, J., Schacter, D., 2008. The brain's default network: anatomy, function, and relevance to disease. *Ann. N. Y. Acad. Sci.* 1124, 1–38.
- Butts, C., 2009. Revisiting the foundations of network analysis. *Science* 325, 414–416.
- Calhoun, V.D., Adali, T., Pearlson, G.D., Pekar, J.J., 2001. A method for making group inferences from functional MRI data using independent component analysis. *Hum. Brain Mapp.* 14, 140–151.
- Chang, C., Glover, G.H., 2010. Time–frequency dynamics of resting-state brain connectivity measured with fMRI. *NeuroImage* 50, 81–98.
- Chen, B., Bouchard, M., McCaslin, F., Burgess, S., Hillman, E., 2011. High-speed vascular dynamics of the hemodynamic response. *NeuroImage* 54, 1021–1030.
- Christoff, K., Gordon, A.M., Smallwood, J., Smith, R., Schooler, J.W., 2009. Experience sampling during fMRI reveals default network and executive system contributions to mind wandering. *Proc. Natl. Acad. Sci. U. S. A.* 106, 8719–8724.
- Corbetta, M., Shulman, G.L., 2002. Control of goal-directed and stimulus-driven attention in the brain. *Nat. Rev. Neurosci.* 3, 201–215.
- Cui, X., Bray, S., Bryant, D.M., Glover, G.H., Reiss, A.L., 2011. A quantitative comparison of NIRS and fMRI across multiple cognitive tasks. *NeuroImage* 54, 2808–2821.
- Cui, X., Bryant, D.M., Reiss, A.L., 2012. NIRS-based hyperscanning reveals increased interpersonal coherence in superior frontal cortex during cooperation. *NeuroImage* 59, 2430–2437.
- D'Argembeau, A., Collette, F., Van der Linden, M., Laureys, S., Del Fiore, G., Degueldre, C., Luxen, A., Salmon, E., 2005. Self-referential reflective activity and its relationship with rest: a PET study. *NeuroImage* 25, 616–624.
- Dagli, M.S., Ingeholm, J.E., Haxby, J.V., 1999. Localization of cardiac-induced signal change in fMRI. *NeuroImage* 9, 407–415.
- Damoiseaux, J.S., Rombouts, S.A., Barkhof, F., Scheltens, P., Stam, C.J., Smith, S.M., Beckmann, C.F., 2006. Consistent resting-state networks across healthy subjects. *Proc. Natl. Acad. Sci. U. S. A.* 103, 13848–13853.
- De Luca, M., Beckmann, C.F., De, S.N., Matthews, P.M., Smith, S.M., 2006. fMRI resting state networks define distinct modes of long-distance interactions in the human brain. *NeuroImage* 29, 1359–1367.
- Devor, A., Tian, P., Nishimura, N., Teng, I., Hillman, E., Narayanan, S., Ulbert, I., Boas, D., Kleinfeld, D., Dale, A., 2007. Suppressed neuronal activity and concurrent arterial vasoconstriction may explain negative blood oxygenation level-dependent signal. *J. Neurosci.* 27, 4452–4459.
- Doria, V., Beckmann, C.F., Arichi, T., Merchant, N., Groppo, M., Turkheimer, F.E., Counsell, S.J., Murgasova, M., Aljabar, P., Nunes, R.G., Larkman, D.J., Rees, G., Edwards, A.D., 2010. Emergence of resting state networks in the preterm human brain. *Proc. Natl. Acad. Sci. U. S. A.* 107, 20015–20020.
- Duan, L., Zhang, Y., Zhu, C., 2012. Quantitative comparison of resting-state functional connectivity derived from fNIRS and fMRI: a simultaneous recording study. *NeuroImage* 60, 2008–2018.
- Fornito, A., Bullmore, E.T., 2010. What can spontaneous fluctuations of the blood oxygenation-level-dependent signal tell us about psychiatric disorders? *Curr. Opin. Psychiatry* 23, 239–249.
- Fox, M.D., Greicius, M.D., 2010. Clinical applications of resting state functional connectivity. *Front. Syst. Neurosci.* 4, 1–13.
- Fox, M.D., Raichle, M.E., 2007. Spontaneous fluctuations in brain activity observed with functional magnetic resonance imaging. *Nat. Rev. Neurosci.* 8, 700–711.
- Fox, M.D., Snyder, A.Z., Vincent, J.L., Corbetta, M., Van Essen, D.C., Raichle, M.E., 2005. The human brain is intrinsically organized into dynamic, anticorrelated functional networks. *Proc. Natl. Acad. Sci. U. S. A.* 102, 9673–9678.
- Fox, M.D., Corbetta, M., Snyder, A.Z., Vincent, J.L., Raichle, M.E., 2006. Spontaneous neuronal activity distinguishes human dorsal and ventral attention systems. *Proc. Natl. Acad. Sci. U. S. A.* 103, 10046–10051.
- Fox, M.D., Zhang, D., Snyder, A.Z., Raichle, M.E., 2009. The global signal and observed anticorrelated resting state brain networks. *J. Neurophysiol.* 101, 3270–3283.
- Fransson, P., 2005. Spontaneous low-frequency BOLD signal fluctuations: an fMRI investigation of the resting-state default mode of brain function hypothesis. *Hum. Brain Mapp.* 26, 15–29.
- Funane, T., Kiguchi, M., Atsumori, H., Sato, H., Kubota, K., Koizumi, H., 2011. Synchronous activity of two people's prefrontal cortices during a cooperative task measured by simultaneous near-infrared spectroscopy. *J. Biomed. Opt.* 16, 077011.
- Gagnon, L., Cooper, R.J., Yücel, M.A., Perdue, K.L., Greve, D.N., Boas, D.A., 2012a. Short separation channel location impacts the performance of short channel regression in NIRS. *NeuroImage* 59, 2518–2528.
- Gagnon, L., Yücel, M.A., Dehaes, M., Cooper, R.J., Perdue, K.L., Selb, J., Huppert, T.H., Hoge, R.D., Boas, D.A., 2012b. Quantification of the cortical contribution to the NIRS signal over the motor cortex using concurrent NIRS–fMRI measurements. *NeuroImage* 59, 3933–3940.
- Gallagher, H.L., Frith, C.D., 2003. Functional imaging of “theory of mind”. *Trends Cogn. Sci.* 7, 77–83.
- Gao, W., Lin, W., 2012. Frontal parietal control network regulates the anti-correlated default and dorsal attention networks. *Hum. Brain Mapp.* 33, 192–202.
- Gao, W., Zhu, H., Giovanello, K.S., Smith, J.K., Shen, D., Gilmore, J.H., Lin, W., 2009. Evidence on the emergence of the brain's default network from 2-week-old to 2-year-old healthy pediatric subjects. *Proc. Natl. Acad. Sci. U. S. A.* 106, 6790–6795.
- Greicius, M.D., Krasnow, B., Reiss, A.L., Menon, V., 2003. Functional connectivity in the resting brain: a network analysis of the default mode hypothesis. *Proc. Natl. Acad. Sci. U. S. A.* 100, 253–258 (19, 72–78).
- Guionnet, S., Nadel, J., Bertasi, E., Sperduti, M., Delaveau, P., Fossati, P., 2012. Reciprocal Imitation: Toward a neural basis of social interaction. *Cereb. Cortex.* 22, 971–978.
- Gusnard, D.A., Akbudak, E., Shulman, G.L., Raichle, M.E., 2001. Medial prefrontal cortex and self-referential mental activity: relation to a default mode of brain function. *Proc. Natl. Acad. Sci. U. S. A.* 98, 4259–4264.
- Hoge, R.D., Franceschini, M.A., Covolan, R.J.M., Huppert, T., Mandeville, J.B., Boas, D.A., 2005. Simultaneous recording of task-induced changes in blood oxygenation, volume, and flow using diffuse optical imaging and arterial spin-labeling MRI. *NeuroImage* 25, 701–707.
- Homae, F., Watanabe, H., Otobe, T., Nakano, T., Go, T., Konishi, Y., Taga, G., 2010. Development of global cortical networks in early infancy. *J. Neurosci.* 30, 4877–4882.
- Homae, F., Watanabe, H., Nakano, T., Taga, G., 2011. Large-scale brain networks underlying language acquisition in early infancy. *Front. Psychol.* 2, 93.
- Huppert, T., Hoge, R., Dale, A., Franceschini, M., Boas, D., 2006a. Quantitative spatial comparison of diffuse optical imaging with blood oxygen level-dependent and arterial spin labeling-based functional magnetic resonance imaging. *J. Biomed. Opt.* 11, 064018.
- Huppert, T., Hoge, R., Diamond, S., Franceschini, M., Boas, D., 2006b. A temporal comparison of BOLD, ASL, and NIRS hemodynamic responses to motor stimuli in adult humans. *NeuroImage* 29, 368–382.
- Kang, J., Wang, L., Yan, C., Wang, J., Liang, X., He, Y., 2011. Characterizing dynamic functional connectivity in the resting brain using variable parameter regression and Kalman filtering approaches. *NeuroImage* 56, 1222–1234.
- Kelly, A.M.C., Uddin, L.Q., Biswal, B.B., Castellanos, F.X., Milham, M.P., 2008. Competition between functional brain networks mediates behavioral variability. *NeuroImage* 39, 527–537.
- Kleinschmidt, A., Obrig, H., Requardt, M., Merboldt, K.D., Dirnagl, U., Villringer, A., Frahm, J., 1996. Simultaneous recording of cerebral blood oxygenation changes during human brain activation by magnetic resonance imaging and near-infrared spectroscopy. *J. Cereb. Blood Flow Metab.* 16, 817–826.
- Kohno, S., Miyai, I., Seiyama, A., Oda, I., Ishikawa, A., Tsuneishi, S., Amita, T., Shimizu, K., 2007. Removal of the skin blood flow artifact in functional near-infrared spectroscopic imaging data through independent component analysis. *J. Biomed. Opt.* 12, 062111.
- Lowe, M.J., Mock, B.J., Sorenson, J.A., 1998. Functional connectivity in single and multislice echoplanar imaging using resting-state fluctuations. *NeuroImage* 7, 119–132.
- Lu, C.M., Zhang, Y.J., Biswal, B.B., Zang, Y.F., Peng, D.L., Zhu, C.Z., 2010. Use of fNIRS to assess resting state functional connectivity. *J. Neurosci. Methods* 186, 242–249.
- Majeed, W., Magnuson, M., Hasenkamp, W., Schwab, H., Schumacher, E.H., Barsalou, L., Keilholz, S.D., 2011. Spatiotemporal dynamics of low frequency BOLD fluctuations in rats and humans. *NeuroImage* 54, 1140–1150.
- Mason, M.F., Norton, M.I., Van Horn, J.D., Wegner, D.M., Grafton, S.T., Macrae, C.N., 2007. Wandering minds: the default network and stimulus independent thought. *Science* 315, 393–395.
- Massimini, M., Ferrarelli, F., Huber, R., Esser, S.K., Singh, H., Tononi, G., 2005. Breakdown of cortical effective connectivity during sleep. *Science* 30, 2228–2232.
- Mesquita, R.C., Franceschini, M.A., Boas, A.A., 2010. Resting state functional connectivity of the whole head with near-infrared spectroscopy. *Biomed. Opt. Express* 1, 324–336.
- Mitchell, J.P., Heatherton, T.F., Macrae, C.N., 2002. Distinct neural systems subserve person and object knowledge. *Proc. Natl. Acad. Sci. U. S. A.* 99, 15238–15243.
- Mitchell, J.P., Macrae, C.N., Banaji, M.R., 2006. Dissociable medial prefrontal contributions to judgments of similar and dissimilar others. *Neuron* 50, 655–663.
- Moussa, M.N., Vechlekar, C.D., Burdette, J.H., Steen, M.R., Huggenschmidt, C.E., Laurienti, P.J., 2011. Changes in cognitive state alter human functional brain networks. *Front. Hum. Neurosci.* 5, 83.
- Murphy, K., Birn, R.M., Handwerker, D.A., Jones, T.B., Bandettini, P.A., 2009. The impact of global signal regression on resting state correlations: are anti-correlated networks introduced? *NeuroImage* 44, 893–905.
- Obrig, H., Neufang, M., Wenzel, R., Kohl, M., Steinbrink, J., Einhaupl, K., Villringer, A., 2000. Spontaneous low frequency oscillations of cerebral hemodynamics and metabolism in human adults. *NeuroImage* 12, 623–639.
- Ogawa, S., Lee, T., Kay, A., Tank, D., 1990. Brain magnetic resonance imaging with contrast dependent on blood oxygenation. *Proc. Natl. Acad. Sci. U. S. A.* 87, 9868–9872.
- Okada, E., Firbank, M., Schweiger, M., Arridge, S., Cope, M., Delpy, D., 1997. Theoretical and experimental investigation of near-infrared light propagation in a model of the adult head. *Appl. Opt.* 36, 21–31.
- Okamoto, M., Dan, H., Sakamoto, K., Takeo, K., Shimizu, K., Kohno, S., Oda, I., Isobe, S., Suzuki, T., Kohyama, K., Dan, I., 2004. Three-dimensional probabilistic anatomical cranio-cerebral correlation via the international 10–20 system oriented for transcranial functional brain mapping. *NeuroImage* 21, 99–111.
- Raichle, M., MacLeod, A., Snyder, A., Powers, W., Gusnard, D., Shulman, G., 2001. A default mode of brain function. *Proc. Natl. Acad. Sci. U. S. A.* 98, 676–682.
- Redcay, E., Dodell-Feder, D., Pearrow, M.J., Mavros, P.L., Kleiner, M., Gabrieli, J.D., Saxe, R., 2010. Live face-to-face interaction during fMRI: a new tool for social cognitive neuroscience. *NeuroImage* 50, 1639–1647.
- Rilling, J.K., Sanfey, A.G., Aronson, J.A., Nystrom, L.E., Cohen, J.D., 2004. The neural correlates of theory of mind within interpersonal interactions. *NeuroImage* 22, 1694–1703.
- Rilling, J.K., Dagenais, J.E., Goldsmith, D.R., Glenn, A.L., Pagnoni, G., 2008. Social cognitive neural networks during in-group and out-group interactions. *NeuroImage* 41, 1447–1461.
- Roche-Labarbe, N., Zaaimi, B., Berquin, P., Nehlig, A., Grebe, R., Wallois, F., 2008. NIRS-measured oxy- and deoxyhemoglobin changes associated with EEG spike-and-wave discharges in children. *Epilepsia* 49, 1871–1880.

- Saager, R.B., Berger, A.J., 2008. Measurement of layer-like hemodynamic trends in scalp and cortex: implications for physiological baseline suppression in functional near infrared spectroscopy. *J. Biomed. Opt.* 13, 034017.
- Saito, D.N., Tanabe, H.C., Izuma, K., Hayashi, M.J., Morito, Y., Komeda, H., Uchiyama, H., Kosaka, H., Okazawa, H., Fujibayashi, Y., Sadato, N., 2010. "Stay tuned": inter-individual neural synchronization during mutual gaze and joint attention. *Front. Integr. Neurosci.* 4, 127.
- Sasai, S., Homae, F., Watanabe, H., Taga, G., 2011. Frequency-specific functional connectivity in the brain during resting state revealed by NIRS. *NeuroImage* 56, 252–257.
- Schacter, D.L., Addis, D.R., Buckner, R.L., 2007. Remembering the past to imagine the future: the prospective brain. *Nat. Rev. Neurosci.* 8, 657–661.
- Schilbach, L., Wilms, M., Eickhoff, S.B., Romanzetti, S., Tepest, R., Bente, G., Shah, N.J., Fink, G.R., Vogeley, K., 2010. Minds made for sharing: initiating joint attention recruits reward-related neurocircuitry. *J. Cogn. Neurosci.* 22, 2702–2715.
- Schroeter, M.L., Kupka, T., Mildner, T., Uludag, K., von Cramon, D.Y., 2006. Investigating the post-stimulus undershoot of the BOLD signal—a simultaneous fMRI and fNIRS study. *NeuroImage* 30, 349–358.
- Spreng, R.N., Mar, R.A., Kim, A.S., 2009. The common neural basis of autobiographical memory, prospection, navigation, theory of mind, and the default mode: a quantitative meta-analysis. *J. Cogn. Neurosci.* 21, 489–510.
- Sridharan, D., Levitin, D.J., Menon, V., 2008. A critical role for the right fronto-insular cortex in switching between central-executive and default-mode networks. *Proc. Natl. Acad. Sci. U. S. A.* 105, 12569–12574.
- Steinbrink, J., Villringer, A., Kempf, F., Haux, D., Boden, S., Obrig, H., 2006. Illuminating the BOLD signal: combined fMRI–fNIRS studies. *Magn. Res. Imaging* 24, 495–505.
- Strangman, G., Culver, J., Thompson, J., Boas, D., 2002. A quantitative comparison of simultaneous BOLD fMRI and NIRS recordings during functional brain activation. *NeuroImage* 17, 719–731.
- Tachtsidis, I., Leung, T., Tisdall, M., Devendra, P., Smith, M., Delpy, D., Ellwell, C., 2008. Investigation of frontal cortex, motor cortex and systemic haemodynamic changes during anagram solving. *Adv. Exp. Biol.* 614, 21–28.
- Taga, G., Konishi, Y., Maki, A., Tachibana, T., Fujiwara, M., Koizumi, H., 2000. Spontaneous oscillation of oxy- and deoxy-hemoglobin changes with a phase difference throughout the occipital cortex of newborn infants observed using noninvasive optical topography. *Neurosci. Lett.* 282, 101–104.
- Taga, G., Watanabe, H., Homae, F., 2011. Spatiotemporal properties of cortical hemodynamic response to auditory stimuli in sleeping infants revealed by multi-channel NIRS. *Phil. Trans. R. Soc. A* 369, 4495–4511.
- Takahashi, T., Takikawa, Y., Kawagoe, R., Shibuya, S., Iwano, T., 2011. Influence of skin blood flow on near-infrared spectroscopy signals measured on the forehead during a verbal fluency task. *NeuroImage* 57, 991–1002.
- Tognoli, E., Lagarde, J., DeGuzman, G.C., Kelso, J.A., 2007. The phi complex as a neuromarker of human social coordination. *Proc. Natl. Acad. Sci. U. S. A.* 104, 8190–8195.
- Tong, Y., Frederick, B., 2010. Time lag dependent multimodal processing of concurrent fMRI and near-infrared spectroscopy (NIRS) data suggests a global circulatory origin for low-frequency oscillation signals in human brain. *NeuroImage* 53, 553–564.
- Tonorov, V., Franceschini, M., Filiaci, M., Fantini, S., Wolf, M., Michalos, A., Gratton, E., 2000. Near-infrared study of fluctuations in cerebral hemodynamics during rest and motor stimulation: temporal analysis and spatial mapping. *Med. Phys.* 27 (4), 801–815.
- Tonorov, V., Webb, A., Choi, J., 2001. Investigation of human brain hemodynamics by simultaneous near-infrared spectroscopy and functional magnetic resonance imaging. *Med. Phys.* 28, 521–527.
- Toyoda, H., Kashikura, K., Ikada, T., Nakashita, S., Honda, M., Yonekura, Y., Kawaguchi, H., Maki, A., Sadato, N., 2008. Source of nonlinearity of the BOLD response revealed by simultaneous fMRI and NIRS. *NeuroImage* 39, 997–1013.
- Tzourio-Mazoyer, N., Landeau, B., Papathanassiou, D., Crivello, F., Etard, O., Delcroix, N., Mazoyer, B., Joliot, M., 2002. Automated anatomical labeling of activations in SPM using a macroscopic anatomical parcellation of the MNI MRI single-subject brain. *NeuroImage* 15, 273–289.
- van de Ven, V.G., Formisano, E., Prvulovic, D., Roeder, C.H., Linden, D.E., 2004. Functional connectivity as revealed by spatial independent component analysis of fMRI measurements during rest. *Hum. Brain Mapp.* 22, 165–178.
- van den Heuvel, M.P., Hulshoff, H.E., 2010. Exploring the brain network: a review on resting-state fMRI functional connectivity. *Eur. Neuropsychopharmacol.* 20, 519–534.
- van den Heuvel, M.P., Mandl, R.C., Hulshoff Pol, H.E., 2008. Normalized group clustering of resting-state fMRI data. *PLoS One* 3, e2001.
- van der Zee, P., Arridge, S., Cope, M., Delpy, D., 1990. The effect of optode positioning on optical pathlength in near infrared spectroscopy of brain. *Adv. Exp. Med. Biol.* 277, 79–84.
- Vincent, J., Patel, G., Fox, M., Snyder, A., Baker, J., van Essen, D., Zempel, J., Snyder, L., Corbetta, M., Raichle, M., 2007. Intrinsic functional architecture in the anaesthetized monkey brain. *Nature* 447, 83–86.
- Vincent, J., Kahn, I., Snyder, A., Raichle, M., Buckner, R., 2008. Evidence for a frontoparietal control system revealed by intrinsic functional connectivity. *J. Neurophysiol.* 100, 3328–3342.
- White, B., Snyder, A., Cohen, A., Petersen, S., Raichle, M., Schlaggar, B., Culver, J., 2009. Resting-state functional connectivity in the human brain revealed with diffuse optical tomography. *NeuroImage* 47, 148–156.
- White, B.R., Liao, S.M., Ferradal, S.L., Inder, T.E., Culver, J.P., 2012. Bedside optical imaging of occipital resting-state functional connectivity in neonates. *NeuroImage* 59, 2529–2538.
- Windischberger, C., Langenberger, H., Sycha, T., Tschernko, E., Fuchsjaeger-Mayerl, G., Schmetterer, L., Moser, E., 2002. On the origin of respiratory artifacts in BOLD-EPI of the human brain. *Magn. Reson. Imaging* 20, 575–582.
- Yamada, T., Umeyama, S., Matsuda, K., 2009. Multidistance probe arrangement to eliminate artifacts in functional near-infrared spectroscopy. *J. Biomed. Opt.* 16 (4), 06434.
- Zhang, Q., Brown, E.N., Strangman, G.E., 2007. Adaptive filtering to reduce global interference in evoked brain activity detection: a human subject case study. *J. Biomed. Opt.* 12, 064009.
- Zhang, H., Zhang, Y., Lu, C., Ma, S., Zang, Y., Zhu, C., 2010. Functional connectivity as revealed by independent component analysis of resting-state fNIRS measurements. *NeuroImage* 51, 1150–1161.
- Zhang, H., Duan, L., Zhang, Y., Lu, C., Liu, H., Zhu, C., 2011. Test–retest assessment of independent component analysis-derived resting-state functional connectivity based on functional near-infrared spectroscopy. *NeuroImage* 55, 607–615.
- Zuo, X.N., Kelly, C., Adelman, J.S., Klein, D.F., Castellanos, F.X., Milham, M.P., 2010. Reliable intrinsic connectivity networks: test–retest evaluation using ICA and dual regression approach. *NeuroImage* 49, 2163–2177.